



The University of Manchester

Investigating The Feasibility Of A Foldable Horn Antenna For A Radio Telescope

A dissertation submitted to The University of Manchester for the degree of
Aerospace Engineering

in the Faculty of Science and Engineering

YEAR OF SUBMISSION

2025

Celestine Dal

11017673

Supervised by Dr. Kate Smith

SCHOOL OF ENGINEERING 2024-25

Contents

List of figures	6
List of tables	6
Nomenclature	7
Abstract	8
Lay summary	9
Declaration	10
Intellectual property statement	10
1 Introduction	11
2 Aim & Objectives	13
3 Literature Review	14
3.1 Design Considerations of Different Types of Horn Antennas	14
3.1.1 Pyramidal Horn Antennas	14
3.1.2 Conical Horn Antennas	15
3.1.3 Corrugated Horn Antennas	16
3.2 Potential Horn Antenna Materials	17
3.3 Types of Origami Folds	18
3.3.1 Miura Folding	18
3.3.2 Kresling Folding	21
3.4 Deployment methods	22
3.5 The Effects of Folding and Creasing	25
4 Methodology	27
4.1 Initial methodology proposal	27
4.2 Final methodology used	28
4.2.1 Creating the Solidworks models	28
4.2.2 Creating FEA simulations	37
4.2.3 Changing the material	39
5 Results	41
5.1 Varying b:a ratio	41
5.2 Varying thickness	43
5.3 Varying material	46

5.4	Uncertainty analysis	48
5.4.1	Mesh element size	48
5.4.2	Material properties	49
6	Discussion	51
6.1	Methodology limitations	51
6.2	Critical analysis of results	53
6.3	Links to broader engineering context	55
7	Conclusion	56
Appendix A		58
Project Plan		58
Initial plan		58
First revised plan		58
Second revised plan		60
Final detailed plan		61
Appendix B		62
Risk management		62
Laptop breaks		62
Issues with lab access		62
No material access		62
Time management		62
References		64

Word count: 9622

List of Figures

3.1	Labelled diagram of a pyramidal horn antenna as viewed in the E plane (left) and H plane (right)	14
3.2	Labelled side view of a conical horn antenna	15
3.3	Labelled side view of a corrugated horn antenna	16
3.4	Unfolded (left) and folded (right) Miura fold from Origami Simulator software	19
3.5	Labelled unit cell of a Miura fold, depicting geometric parameters (Schenk and Guest 2013)	19
3.6	Crease pattern of a unit cell for an arc-Miura pattern (Wang et al. 2024)	20
3.7	Tessellated pattern (left) and fully folded state (right) of an arc-Miura folded model (Wang et al. 2024)	20
3.8	Kresling folds for different Gaussian curvatures, showing folded and deployed state (Lu et al. 2021)	21
3.9	Single story depiction of Kresling fold, with geometric parameter labels (Moshtaghzadeh et al. 2022)	21
3.10	Labelled cross-section of a folded metal edge (Walker and Seffen 2018) . .	25
4.1	Huffman waterbomb pattern from Origami Simulator software, visualises strain	27
4.2	Setting fold angle and b dimensions	29
4.3	Sketched construction lines	29
4.4	Creating a reference plane	30
4.5	Sketching the first parallelogram panel	30
4.6	Creating a construction line for reference	31
4.7	Creating the second reference plane	31
4.8	Sketching the second parallelogram panel	32

4.9	Creating three reference planes for thickness sketches	32
4.10	Sketching the cross section of the panel	33
4.11	All thickness sketches created	33
4.12	Creating a loft to produce a solid body	34
4.13	Creating the second loft	34
4.14	Mirroring the model to create one Miura unit cell	35
4.15	Linear patterning the Miura unit cell in the right plane	35
4.16	Linear patterning four Miura unit cells in the front plane	36
4.17	Final result for model 1	36
4.18	Setting fixture panels	38
4.19	Setting the force applied on the panels	38
4.20	Creating the mesh	39
4.21	Defining the material properties	40
5.1	Model 1 results: 3mm thick foamboard and 1:1 ratio	41
5.2	Model 2 results: 3mm thick foamboard and 1:2 ratio	41
5.3	Model 3 results: 3mm thick foamboard and 1:1.5 ratio	42
5.4	Model 4 results: 3mm thick foamboard and 2:1 ratio	42
5.5	Model 5 results: 3mm thick foamboard and 1.5:1 ratio	43
5.6	Model 6 results: 1mm thick foamboard and 1:1 ratio	43
5.7	Model 7 results: 2mm thick foamboard and 1:1 ratio	44
5.8	Model 8 results: 5mm thick foamboard and 1:1 ratio	44
5.9	Model 9 results: 10mm thick foamboard and 1:1 ratio	45
5.10	Model 10 results: 20mm thick foamboard and 1:1 ratio	45
5.11	Model 11 results: 1mm thick Nitinol and 1:1 ratio	46

5.12	Model 12 results: 1mm thick PEEK and 1:1 ratio	46
5.13	Model 13 results: 1mm thick Kapton and 1:1 ratio	47
5.14	Model 14 results: 1mm thick CFRP and 1:1 ratio	47
5.15	Mesh convergence as a result of mesh refinement	49
7.1	Initial gantt chart created in week 2	58
7.2	Project proposal gantt chart with clearer work packages and detailed due dates for project deliverables	59
7.3	Gantt chart for other module deadlines for semester 1	59
7.4	Spreadsheet detailing number of hours to spend vs number of hours actually spent on work packages every week and includes notes to explain deviations from expected hours (to be updated weekly)	60
7.5	Second revised plan created in week 17	60
7.6	Final detailed plan created at the end of the project	61

List of Tables

4.1	Chosen geometry ratios and their corresponding parallelogram side lengths (a) and model heights (H)	37
5.1	Material properties for Nitinol (Alipour et al. 2022), PEEK (Skirbutis et al. 2018), Kapton (Alarcón López 2017) and CFRP (Kumar, R. Singh, and Sharma 2021)	48
5.2	Mesh element size used for models and their corresponding maximum stress values and calculated sensitivity index	49
5.3	Uncertainty in material properties with sensitivity index shown for maximum stress values	50

Nomenclature

ϵ_{ap}	Aperture efficiency
λ	Wavelength
λ_c	Cutoff wavelength
a_j	Radius of corrugated horn antenna
d_j	Slot depth
E	Young's modulus
J_1	Bessel function of the first kind
k_c	Cutoff wavenumber
N	Poisson's ratio
n	Number of polygon sides
Y_1	Bessel function of the second kind

Abstract

There are currently no examples in industry of a foldable horn antenna for use on a radio telescope, due to limitations caused by size requirements but also creases and imperfections formed during the folding and deployment stages of many researched and tested materials. This individual project aims to assess the feasibility of an origami inspired solution through finite element analysis simulations on Solidworks and designing and making foldable horn antenna models to be tested. Horn antennas used at low frequencies need to be very large which can clash with volume and fuel constraints, hence the need to be folded up during launch into space.

Origami-inspired models were created by optimising the Miura unit cell pattern and for each model, geometry, thickness and material was varied in order to produce stress, strain and displacement plots in Solidworks by simulating deployment from a folded state. The results demonstrated that smart materials with properties desirable for horn antennas, such as high conductivity or good corrosion resistance can feasibly be folded into a compact Miura folded design, presenting the opportunity for more passive or automated deployment methods to be developed. The FEA analysis done on this specific 3D pattern enabled the comparison of failure modes and fatigue, facilitating the identification of chosen material for a specific mission's system requirements.

In future, the concepts tested in this report will be transferred to practical experiments, enabling a more accurate approach to testing different deployment methods for Miura folded structures.

Lay summary

Detecting signals in space can sometimes require large antennas that are too big to fit in a rocket and they therefore need to be folded up, launched into space and unfolded when they get there. This project used the concept of origami to make and test foldable structures to see how different materials and thicknesses compared. It was found that certain materials remained strong during unfolding, suggesting a practical solution for a folded antenna that would still ensure a cost effective and efficient space mission. The next steps would include physically recreating these simulations to be able to see how factors such as creasing during folding and durability affect the performance of models.

Declaration

I hereby declare that this dissertation is my own original work unless referenced clearly to the contrary. No portion of the work referred to in this dissertation has been submitted in support of an application for another degree or qualification of this or any other university or other institute of learning.

Intellectual property statement

- i. The author of this dissertation (including any appendices and/or schedules to this dissertation) owns certain copyright or related rights in it (the “Copyright”) and she has given The University of Manchester certain rights to use such Copyright, including for administrative purposes.
- ii. Copies of this dissertation, either in full or in extracts and whether in hard or electronic copy, may be made only in accordance with the Copyright, Designs and Patents Act 1988 (as amended) and regulations issued under it or, where appropriate, in accordance with licensing agreements which the University has entered into. This page must form part of any such copies made.
- iii. The ownership of certain Copyright, patents, designs, trademarks and other intellectual property (the “Intellectual Property”) and any reproductions of copyright works in the dissertation, for example graphs and tables (“Reproductions”), which may be described in this dissertation, may not be owned by the author and may be owned by third parties. Such Intellectual Property and Reproductions cannot and must not be made available for use without the prior written permission of the owner(s) of the relevant Intellectual Property and/or Reproductions.
- iv. Further information on the conditions under which disclosure, publication and commercialisation of this dissertation, the Copyright and any Intellectual Property and/or Reproductions described in it may take place is available in the University IP Policy, in any relevant Dissertation restriction declarations deposited in the University Library, and The University Library’s regulations.

1 Introduction

A typical horn antenna has the shape of a pyramidal frustum and they are used to transmit and receive electromagnetic waves, proving to be useful for missions involving satellite communication (Soares, Pinho, and Wuensche 2014) in the microwave region. They can operate over a range of different frequencies which is a factor that greatly affects their size, as a lower frequency corresponds to a longer wavelength. This leads to a need for a very large horn antenna for use in missions involving the lower frequency end of the electromagnetic spectrum, like radio waves and this can be an issue due to volume and fuel constraints of the project and launch.

Low mass and low volume space structures are favourable, as they reduce fuel costs and take up less space in the payload fairing, resulting in cheaper, more efficient missions. Because of this, overcoming the issue of size is a crucial step for minimising costs and volume usage associated with lower frequency projects and this is where the concept of origami can be applied. Folding a horn antenna with the condition of unfolding during deployment in space implies a physical solution, however, how would creases and folds affect the results produced by the fully deployed antenna- if at all? How would a novel foldable solution compare to current, non-origami related solutions? There are many factors that have been considered for current solutions through experiments and research, for example materials (Beyer, Figler, and Owen 2023), shape (Xia et al. 2023) and type of antenna (Grosvenor et al. 2007), all of which will be discussed in more detail in later sections.

Horn antennas have now been around for over eight decades and have several applications, most notably allowing us to understand the origins of the universe- the Holmdel horn antenna (Penzias and Wilson 1964) is credited with the detection of cosmic microwave background radiation and this revealed direct evidence for the Big Bang Theory. Without horn antennas, we would not be able to see through cosmic dust clouds or detect very weak, distant signals in space, which would make precisely mapping and understanding the universe impossible.

The impact of the research of this project to industry is large, as there is a lack of evidence of foldable horn antennas being used for space applications that are capable of doing high precision radio measurements, whilst being lightweight, rigid and

economically feasible to manufacture. The development of a foldable horn antenna through analysis of effects of material use and folding technique would facilitate major advancements in our ability to produce portable, modular and efficient horn antennas.

2 Aim & Objectives

Aim: The aim of this individual project is to assess the feasibility of having a folded horn antenna for a radio telescope.

Objectives:

1. Examine and identify the advantages and limitations of having a folded antenna.
2. Compare the stresses and strains created by different origami tessellation patterns.
3. Evaluate the effects of different suitable materials on antenna folding.
4. Conduct practical experiments to assess folding ability of different models.

3 Literature Review

This section will provide a background to the topic area and wider field, based on previous research, to fill in knowledge gaps. It details all relevant aspects of the project to lay the foundations of achieving the objectives set in Section 2.

3.1 Design Considerations of Different Types of Horn Antennas

There are many types of horn antennas used in industry and in this subsection of the literature review, the three most commonly used shapes will be discussed: Pyramidal, Conical and Corrugated.

3.1.1 Pyramidal Horn Antennas

Pyramidal horn antennas can be flared in both the H-plane and E-plane, as pictured in Figure 3.1, with the H-plane parallel to the magnetic field and the E-plane parallel to the electric field of the electromagnetic wave that is interacting with the antenna.

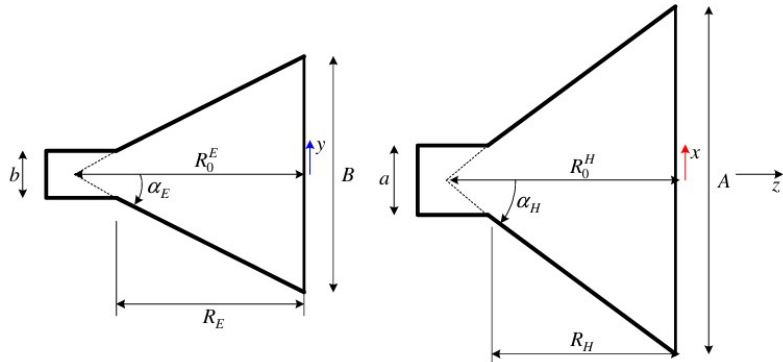


Figure 3.1: Labelled diagram of a pyramidal horn antenna as viewed in the E plane (left) and H plane (right)

Physically, R_E must equal R_H and from Figure 3.1,

$$\frac{R_0^H}{R_H} = \frac{A}{A - a} \quad (3.1)$$

$$\frac{R_0^E}{R_E} = \frac{B}{B - b} \quad (3.2)$$

The gain of this horn antenna is expressed as:

$$G = \frac{4\pi}{\lambda^2} \epsilon_{ap} AB \quad (3.3)$$

From this, (Nikolova n.d.) derived Equation (3.4) as the optimal design equation for this type of horn antenna, which can be solved numerically.

$$A^4 - aA^3 + \frac{3bG\lambda^2}{8\pi\epsilon_{ap}}A - \frac{3G^2\lambda^4}{32\pi^2\epsilon_{ap}^2} = 0 \quad (3.4)$$

System requirements of a project will define parameters of the pyramidal horn antenna such as gain and wavelength, allowing engineers to directly obtain a value for the length A, pictured in Figure 3.1. Substituting into equations (3.1), (3.2) and (3.3) gives the remaining accurate dimensions of the antenna, a crucial step in the design phase. Designs including fold lines and fold angles can then be built off of these core dimensions.

3.1.2 Conical Horn Antennas

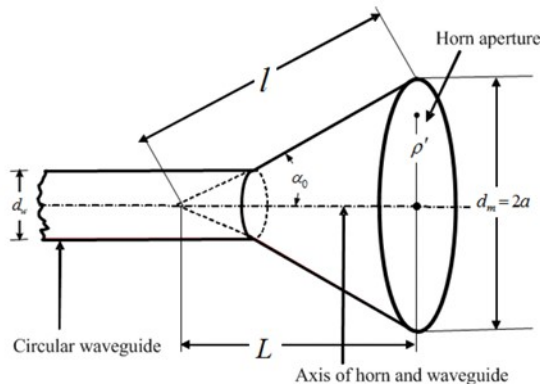


Figure 3.2: Labelled side view of a conical horn antenna

This type of horn antenna (see Figure 3.2) is in the shape of a cone and its dimensions can be optimised (J. Singh and Dhaliwal 2011) by calculating the maximum values of gain (3.5) and directivity imposed by the frequency of the electromagnetic wave that is interacting with the antenna.

$$G = \left(\frac{\pi d_m}{\lambda} \right)^2 \epsilon_{ap} \quad (3.5)$$

The optimal axial length of a conical horn antenna (Aboserwal 2014) can be expressed as:

$$L = 0.3232 \left(\frac{d_m}{\lambda} \right)^2 - 0.0475 \left(\frac{d_m}{\lambda} \right) + 0.0052 \quad (3.6)$$

In the same way as for the pyramidal horn antenna, the optimal design equation (3.6) provides a design solution that will ensure good performance and compactness based on the system requirements of the mission. From this, origami-based iterations can be designed.

3.1.3 Corrugated Horn Antennas

This type of horn antenna can be pyramidal or conical in shape but its distinctive feature is the internal ridges (see Figure 3.3). These ridges, or corrugations, lead to an increase in symmetry in the radiation pattern and they also reduce the effect of cross-polarisation (Gupta 2014), leading to less signal degradation and errors.

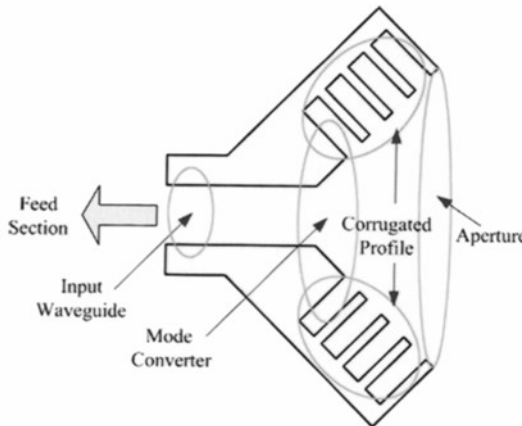


Figure 3.3: Labelled side view of a corrugated horn antenna

Slot depth of the ridges is a significant aspect of the design considerations for corrugated horn antennas and can be expressed for both pyramidal and conical types as follows (Granet and James 2005):

$$X_i = -\delta \frac{J_1(k_c a_j) Y_1(k_c(a_j + d_j)) - Y_1(k_c a_j) J_1(k_c(a_j + d_j))}{J_1(k_c a_j) Y_1(k_c(a_j + d_j)) - Y_1(k_c a_j) J_1(k_c(a_j + d_j))} \quad (3.7)$$

In Equation (3.7), $k_c = \frac{2\pi}{\lambda_c}$. These ridges create an added layer of complexity when

designing and manufacturing a foldable model, however they significantly improve performance of horn antennas for applications such as use for telescopes.

Conclusion: In this subsection of the literature review, types of horn antennas and their optimisation parameters have been discussed. From experiments, researchers have derived equations that make designing these antennas easier. However, some of them require extremely accurate measurements of variables that are beyond the scope of this project. Bearing this in mind, simpler models of these horn antennas shall be made and tested as part of the design and experimental phase of this dissertation.

3.2 Potential Horn Antenna Materials

The vast majority of manufactured horn antennas that have been used for space missions are made out of metals like aluminium, copper and steel or carbon-based composite materials, for example the Holmdel horn antenna was constructed out of aluminium (Crawford, Hogg, and Hunt 1961). This is due to the rigidity requirement of these types of antennas, as well as the need for good electrical conductivity.

This subsection will discuss other materials that have been tested as part of a dynamic folding solution that are yet to be implemented on a large scale for horn antennas operating at low frequencies in space.

The following materials have been used in research projects to achieve a self-folding 3D structure after starting from a 2D or compressed component, which coincides with the aim of this project:

- **Nitinol** (Kshirsagar et al. 2023): This is a nickel-titanium alloy that is classed as a shape memory alloy (SMA) and it is activated by the application of heat. The advantages of using this material in space include its high corrosion resistance and therefore its ability to withstand the harsh environment, as well as the prospect of a self-folding mechanism.
- **PEEK (Polyetheretherketone)** (Kalra et al. 2019): This is a polymer that has several properties that make it ideal for use in space, including its low density (reduces the weight of the payload and in turn, fuel costs) and stability, despite being exposed to space-like vacuum conditions.

- **Kapton** (Wei et al. 2018): This is a polymer film and its use in environments like space is becoming more frequent, due to its good dielectric strength (increases bandwidth for a horn antenna) and mechanical stability.
- **CFRP (Carbon Fibre Reinforced Plastic)** (Wagner and Braun 1980): This is a composite material that is an excellent electrical conductor, allowing good electromagnetic wave reception. CFRPs also offer a high strength to weight ratio, providing the necessary rigidity for foldable horn antenna structures.

Conclusion: Materials used to make horn antennas have many requirements, including good strength to weight ratio, high rigidity, smooth surfaced, good electrical conductivity and the ability to survive the harsh space environment. Researchers have looked into moving away from the usage of the standard metals for horn antennas in order to simplify folded solutions by adding the concept of automation. Although SMAs and SMPs have the advantage of folding and deploying themselves, there are limitations, as researchers have discovered, that override the possibility of application of these materials to a horn antenna. None of the materials mentioned in this subsection other than CFRPs have a higher strength to weight ratio than the current metals used, which is a crucial property to consider for this project.

3.3 Types of Origami Folds

Although many different types of origami folds exist, they are all variations that stem from either Miura or Kresling folding patterns. This subsection will cover both of these, detailing their optimisation and applications to horn antennas.

3.3.1 Miura Folding

Miura folds are a tessellation pattern of parallelograms, as shown in Figure 3.4:

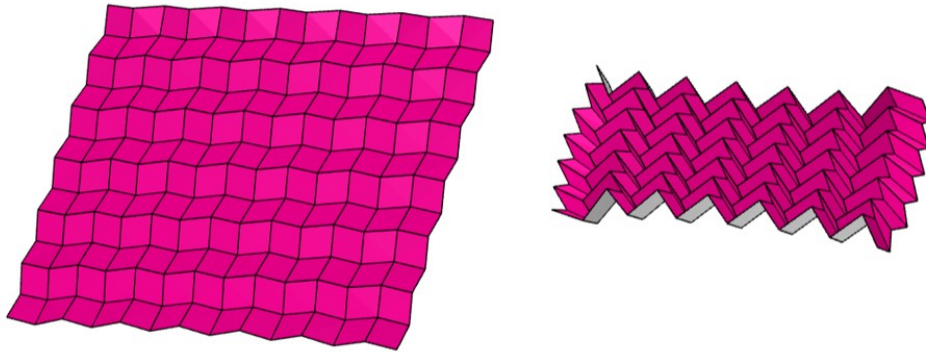


Figure 3.4: Unfolded (left) and folded (right) Miura fold from Origami Simulator software

Being able to parametrise the geometry of this fold is key to understanding the chosen material's mechanical properties and it also offers a means of predicting the physical behaviour of this material. In order to do this, Figure 3.4 (left) must be broken down into a unit cell (see Figure 3.5) which can be described by the following equations:

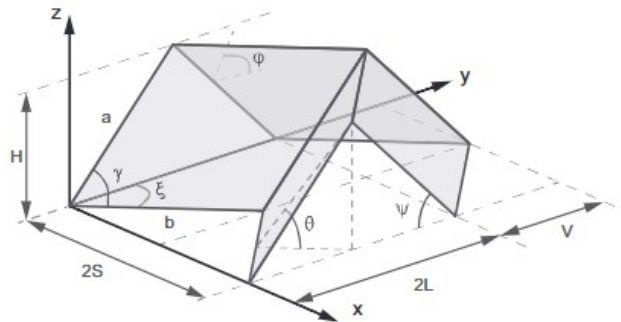


Figure 3.5: Labelled unit cell of a Miura fold, depicting geometric parameters (Schenk and Guest 2013)

$$H = a \sin \theta \sin \gamma \quad (3.8)$$

$$S = b \frac{\cos \theta \tan \gamma}{\sqrt{1 + \cos^2 \theta \tan^2 \gamma}} \quad (3.9)$$

$$L = a \sqrt{1 - \sin^2 \theta \sin^2 \gamma} \quad (3.10)$$

$$V = b \frac{1}{\sqrt{1 + \cos^2 \theta \tan^2 \gamma}} \quad (3.11)$$

These equations shall be used in the Methodology section to ensure accurate creation of models. Folded panels could be combined to create the net of a pyramidal horn antenna. However, in order to achieve a conical shape the panels in the tessellation

pattern must be designed as shown in Figure 3.6:

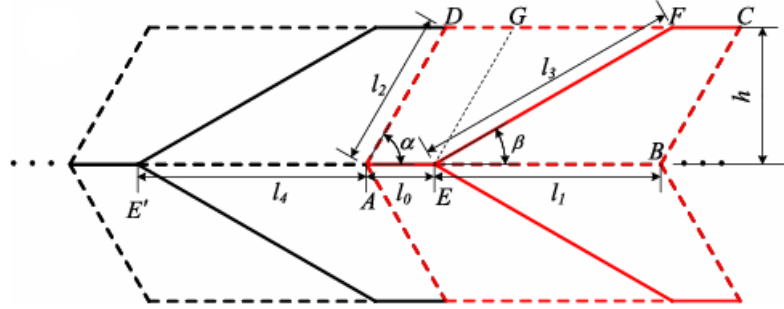


Figure 3.6: Crease pattern of a unit cell for an arc-Miura pattern (Wang et al. 2024)

This design can be parametrised by the following equations:

$$l_{EG} = l_2 = h/\sin\alpha \quad (3.12)$$

$$l_{EF} = l_3 = h/\sin\beta \quad (3.13)$$

$$l_{FG} = l_1 - l_0 \quad (3.14)$$

$$l_0 = l_1 - l_2(\sin\alpha\cot\beta - \cos\alpha) \quad (3.15)$$

The inputs to these equations can be modified and refined until the desired conical shape is achieved (see example in Figure 3.7):

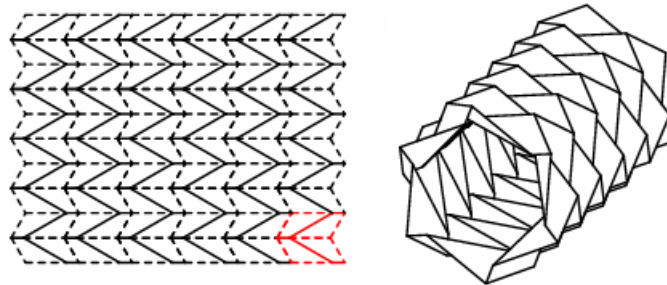


Figure 3.7: Tessellated pattern (left) and fully folded state (right) of an arc-Miura folded model (Wang et al. 2024)

The Miura folding technique has a negative Poisson's ratio and it can easily be applied to deployable horn antennas because it has just one degree of freedom, meaning the mechanism required to collapse the flat pattern only needs to act in one direction on one plane, simplifying deployment.

3.3.2 Kresling Folding

The Kresling folding pattern is another key branch of origami folding techniques, however, instead of tessellations, it involves symmetrical angled folds and is limited to expansion and contraction along one axis, as shown in Figure 3.8:

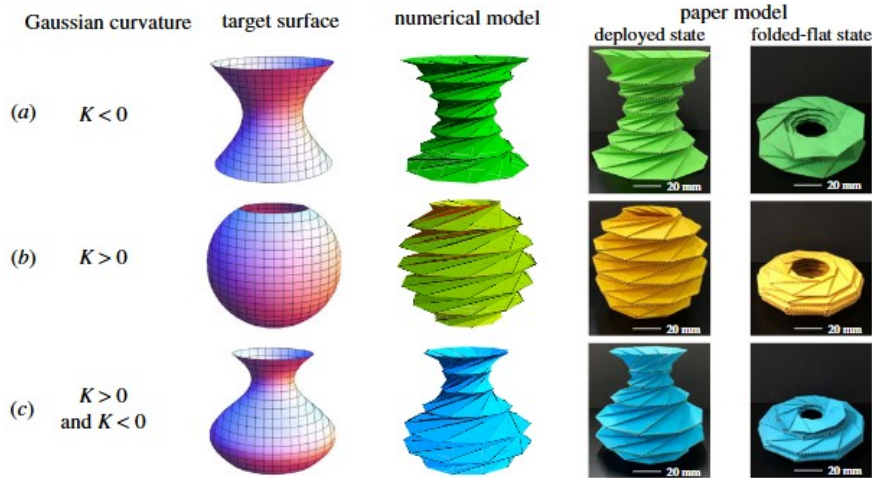


Figure 3.8: Kresling folds for different Gaussian curvatures, showing folded and deployed state (Lu et al. 2021)

A parametrisation of the geometry of this folding technique is detailed in Figure 3.9 and as follows:

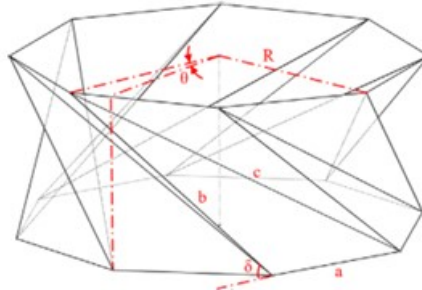


Figure 3.9: Single story depiction of Kresling fold, with geometric parameter labels (Moshtaghzadeh et al. 2022)

$$R = \frac{\frac{a}{2}}{\sin\left(\frac{\pi}{n}\right)} \quad (3.16)$$

$$h = b \sin \delta \quad (3.17)$$

$$b = \sqrt{\left[2R \sin\left(\frac{2\pi/n - \theta}{2}\right)\right]^2 + (b \sin \delta)^2} \quad (3.18)$$

$$\theta = \frac{2\pi}{n} - 2 \arcsin \frac{b \cos \delta}{2R} \quad (3.19)$$

$$c = \sqrt{\left[2R\sin\left(\frac{\pi}{n} + \arcsin\frac{b\cos\delta}{2R}\right)\right]^2 + (b\sin\delta)^2} \quad (3.20)$$

This pattern offers stiffness and rigidity, as well as a single degree of freedom deployable solution. It is much more complex than Miura folding, however, as pictured in Figure 3.9, it would be able to achieve horn antenna shapes discussed in earlier chapters out of a singular piece of material. The elimination of joining processes is favourable for antenna designs, as will be considered in the next subsection.

Conclusion: This subsection explored the two main types of origami folding and their parametrisation (which shall be applied when creating more complex models on Solidworks in Section 4). It suggests two ways that a horn antenna can be folded and the advantages and limitations of these two origami techniques will be assessed later on in the experimental phase of this project.

3.4 Deployment methods

There are many examples in literature of deployment mechanisms used for space structures and this subsection of the literature review will outline and critically analyse different approaches of the main types of deployment methods that are applicable to foldable horn antennas:

- **Elastic flexure deployment** (Hunter, Vijayachandran, and Waas 2023): With this method, hinges are manufactured using viscoelastic material, allowing the hinge to store strain energy when the model is folded. In order to unfold into the desired configuration, this stored energy is simply released. The advantages of this method are that power is not required to achieve deployment and there are no moving parts (the key theme throughout this paper was the application of this hinge type to monolithic structures)- this results in a simple, reliable design and requires less manufacturing. Limitations include the risk of large frictional forces overriding the stored strain energy, preventing deployment or constant folding and unfolding causing fatigue in the hinge material, which will be mentioned in the following subsection.

- **SMA actuation:** As mentioned in the materials subsection of this literature review, shape memory alloys could be used for foldable horn antennas. (Seigner et al. 2020) have used NiTi films as microactuators, which when heated to 60°C, have the ability to fold back to 10°. Similar to the elastic flexure method, one advantage of this method is that it is compact and lightweight, with no extra complex components. The main limitation of this method is that it requires the application of heat, which will increase the total power requirements of the mission.
- **Mechanical spring deployment** (Morgan, Magleby, and Howell 2016): This method of deployment is achieved by storing mechanical energy in springs and its release leads to quick deployment. Although this method is simple and fast, it might be difficult to control short period deployment. Another limitation is that it is difficult to restore the mechanical energy in the springs once they have been released, meaning this is not a reversible method, unlike the previous two.
- **Motorised deployment** (T. P. G. Singh et al. 2024): This common method uses motors or actuators to cause folding and unfolding of the structure. An important advantage is that deployment can be paused or reset at any point and this provides the user with significant autonomy over the system, as each step can be programmed. However, the addition of components adds a layer of complexity to the system which increases the number of failure modes. Another limitation is that this method also requires power and overall, will increase both mass and power budgets of the mission.
- **Inflatable deployment** (Li et al. 2023): This method essentially inflates the folded model using internal pressure to achieve axial expansion and therefore full deployment. This allows the folded model to be very compact because the structure can be unfolded from any state, offering high packing efficiency. A crucial limitation to this method is that the model needs to be rigidised after deployment, which requires a trade off between high stiffness and low thermal expansion. It is also difficult to control this inflation and could lead to punctures in certain materials.
- **Centrifugal deployment** (Okuzumi and Yamamoto 2009): For this method,

thrusters are used to spin the spacecraft, generating centripetal force which unfolds the model. This force is evenly distributed across all panels of the model, resulting in simple, even deployment. Another advantage of this method is that there is no need to manufacture extra components, significantly reducing its complexity. A limitation to this is that it is very difficult to control- spinning could lead to instability, which would be a challenge to regulate or stop precisely.

- **Tensioned cable deployment** (Ma et al. 2021): Similar to the motorised deployment method, this method has the advantage of enabling controlled deployment through the sequential application of tension in cables placed on panels of the structure, or in the case of the cited research paper, as part of a tensegrity dome. There are however several limitations to this theoretical model, namely the intricacy of this method introduces higher risk of failure without redundancy, as there are many moving parts.
- **Origami-creased passive deployment** (Deleo et al. 2020): This method is the only fully passive method and it uses composite materials like CFRP, on which origami crease patterns can be laser cut. The model is folded and cured, embedding a guide for deployment, which will occur as a result of an environmental trigger such as a small vibration. This method is ideal for space applications because it does not require any power or actuation, making it highly reliable. The use of materials such as CFRP offers the model a high strength to weight ratio and they can endure the effects of the harsh space environment. A major limitation is that once the structure has been deployed, there is no way of reversing this process unless other mechanisms are added. The manufacturing of the hinges is an involved process and there must be a trade off between durability and rigidity to ensure that upon deployment, the material provides enough stiffness for the structure to hold its shape without manual assistance.

Conclusion: There are a wide range of deployment mechanisms and the use of many depend on the overall mission and its system requirements because active deployment adds to the mass and power budgets, which is a limitation. Other methods such as origami-creased deployment and SMA actuation mainly depend on the material chosen, rather than having complex additional parts and more failure modes.

3.5 The Effects of Folding and Creasing

In order to remove the complexities of having a large number of intricate hinges and individual surface deployment mechanisms, it is more desirable to simply have a boom or telescopic mast to unfold the horn antenna. This still does not remove the issue of creasing the material during folding and unfolding. Different materials will exhibit different behaviours as a result of stresses encountered during deployment.

When modelling the stresses and strains caused by the folding of materials, the assumption of a thin-walled structure is invalid, as the metals that are used to make horn antennas need to have enough thickness to maintain structural stability and rigidity, therefore a thick fold can be modelled as shown in Figure 3.10:

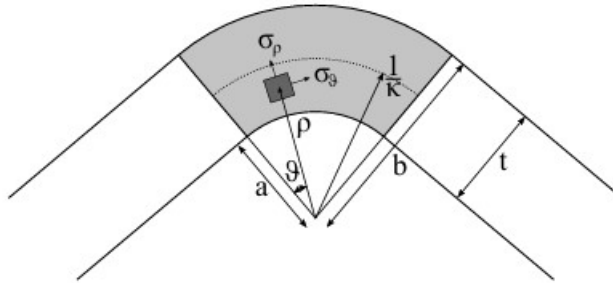


Figure 3.10: Labelled cross-section of a folded metal edge (Walker and Seffen 2018)

The stress produced by folding the material can be analysed using software such as Abaqus or Solidworks and the applied strain can be pictured using Origami Simulator but the stresses can also be expressed using mathematical formulae (Walker and Seffen 2018):

$$\sigma_p = \frac{Et^3}{3N} \left(\frac{1}{r} - \kappa \right) \left(\frac{a^2 b^2 \log \frac{b}{a}}{\rho^2} + a^2 \log \frac{a}{\rho} + b^2 \log \frac{\rho}{b} \right) \quad (3.21)$$

$$\sigma_\theta = \frac{Et^3}{3N} \left(\frac{1}{r} - \kappa \right) \left(-\frac{a^2 b^2 \log \frac{b}{a}}{\rho^2} + a^2 \log \frac{a}{\rho} - a^2 + b^2 \log \frac{\rho}{b} + b^2 \right) \quad (3.22)$$

$$N = \left(b^2 - a^2 \right)^2 - 4a^2 b^2 \log^2 \left(\frac{b}{a} \right) \quad (3.23)$$

These equations allow engineers to predict whether the material used will be strong enough to withstand these stresses and strains, however, even if it can, the other major issue with folding a horn antenna would be the formation of creases or imperfections

in what should be a perfectly smooth surface. This can lead to a decline in the overall performance of the antenna, examples including (Caldecott et al. 1973):

- Random creases and imperfections along the antenna's walls can cause unpredictable reflecting of the electromagnetic waves, resulting in reduced efficiency.
- The less smooth the surface is, the more energy loss occurs, which in turn distorts the radiation pattern.
- Folds may cause the material to become more rough and uneven when folded and unfolded many times. Any minuscule change in geometry can greatly affect the gain and directivity of the antenna, reducing accuracy and consistency of the results obtained.

Conclusion: Naturally, when folding a material, creases and imperfections will form and this has negative consequences for horn antennas (as detailed in this subsection). Researchers have also derived formulae to help engineers predict failure and stresses in certain materials, which will be useful when designing and making foamboard models of foldable horn antennas. The aim of this project is to investigate the feasibility of creating a foldable solution, despite its limitations.

4 Methodology

4.1 Initial methodology proposal

¹One area of importance for this project is the effect of stresses and strains on folding certain materials. Different folding patterns will induce failure or high stress and strain at different parts of the horn antenna. In order to have an initial visualisation of this without spending time and resources on making and testing practical models, software like Origami Simulator were used, as in Figure 4.1. Patterns were inputted to result in the simulation of the actual folding and although this did not produce high level data, parameters such as axial stiffness, fold stiffness and facet crease stiffness could be changed which will effect decision making when creating real, higher level models.

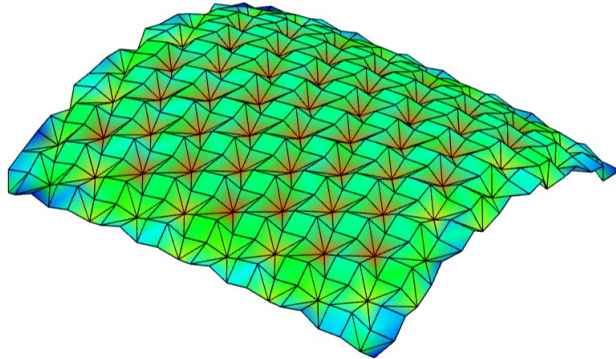


Figure 4.1: Huffman waterbomb pattern from Origami Simulator software, visualises strain

Once a better understanding of the relationship between folding and strain has been attained, scaled models of these folds shall be designed and constructed out of foamboard. This material will be used, as it is cost effective, readily available and easy to cut and bend. It will require minimal equipment and manufacturing time, which is ideal for projects where many quick and simple prototypes need to be made. These models can then be tested on an existing rig in the George Begg building that has been used for similar applications in the past, where the models will undergo physical tests to see how well the folding mechanisms work.

In order to more effectively complete the project objectives, the corresponding

¹See Appendix A for reason for difference between initial and final methodologies

Solidworks models will also be created and a stress analysis shall be performed using the simulation feature of this software. In order to achieve accurate Solidworks models, the sheet metal feature will also be used, which creates folded and unfolded 3D objects. This will replicate the actual models because it will replace perfectly sharp edges with curved edges where the models have been folded. Using the software Solidworks, the simulation of applying force on models made of different materials will produce stress data. This data can then be compared for different origami patterns and it will give an indication of which materials are more suitable for this application, as this property can be easily varied on Solidworks.

Throughout the experimental part of this individual project, a new methodology may be developed or more detail may be added to this methodology if other methods of data collection are required, however this is the initial experimental proposal.

4.2 Final methodology used

This section will detail how the final Solidworks models were made and the steps taken to produce results. In order to replicate the following procedure, basic knowledge of the main elements of the Solidworks user interface is required. The dependent variable for the first five models was the length and height of each parallelogram in a Miura unit cell and for the next five models, it was the thickness. The results section will detail the reason for the choice of the most feasible model out of the first ten created. Once this decision was made, different relevant materials were applied to this model in Solidworks and the stresses and strains were obtained.

4.2.1 Creating the Solidworks models

During the creation of these models, factors such as fold angle and parallelogram geometry were considered (these have been detailed in section 3.3.1). The following example is for the initial model created:

First, the top plane was selected and sketched on as shown in Figure 4.2. The ‘Line’ tool, followed by the ‘Smart Dimension’ tool was used to create a line 200mm long. This value will produce a scaled model for prototyping purposes. This line was

then mirrored in the right plane using the ‘Mirror Entities’ tool. A horizontal line (the ‘For Construction’ option was selected) can be created at the base of the formed ‘v’ shape to ease visualisation later on. The ‘Smart Dimension’ tool was used to ensure a 20° angle between the two solid lines - this corresponds to the fold angle (2ξ).

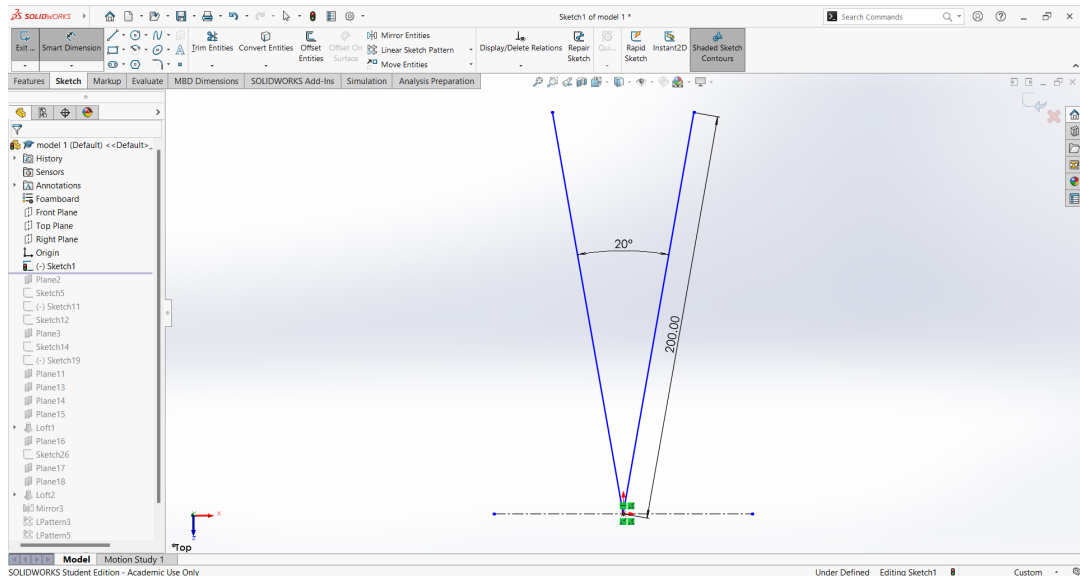


Figure 4.2: Setting fold angle and b dimensions

The right plane was selected and using the ‘Line’ tool in construction mode, a triangle with a 200mm hypotenuse and 100mm base was sketched, as pictured in Figure 4.3.

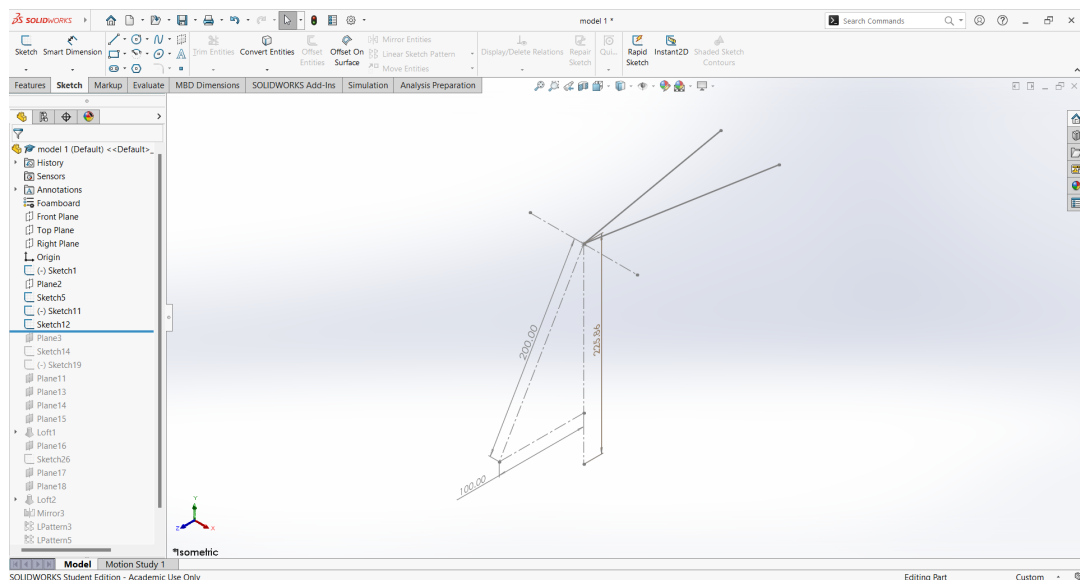


Figure 4.3: Sketched construction lines

In the ‘Features’ section of the ‘Command Manager’, ‘Plane’ was selected from ‘Reference Geometry’. The lines shown in Figure 4.4 were selected in order to create the correct reference plane.

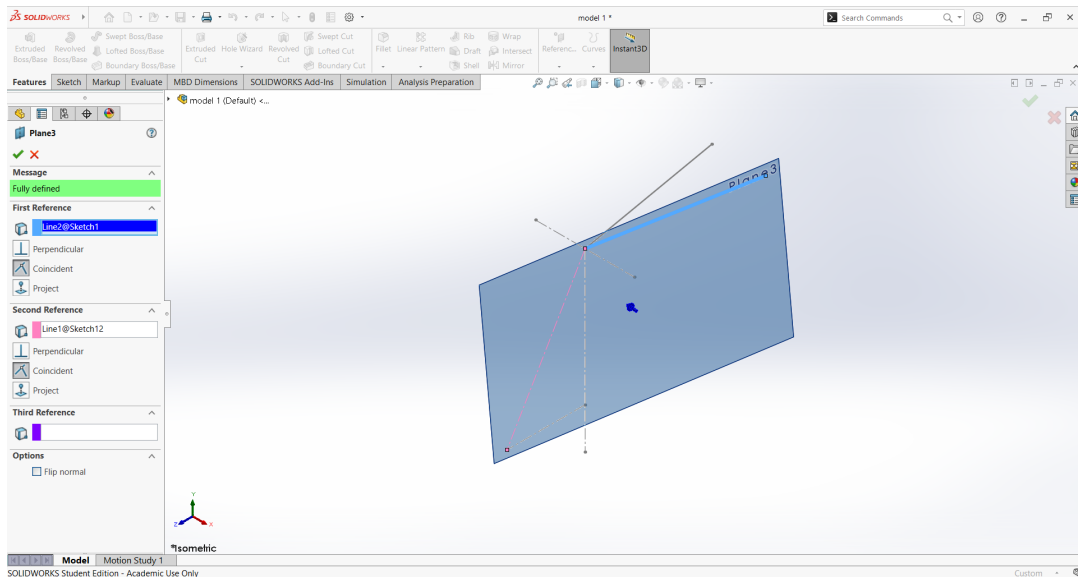


Figure 4.4: Creating a reference plane

This newly created plane was then selected and a sketch was created on it. This sketch forms the shape of one panel in the Miura unit cell tessellation (see Figure 3.5), with each side measuring 200mm and $\gamma = 60^\circ$, as outlined in section 3.3.1. Both pairs of opposite edges were selected and the ‘Parallel’ relation was added to fix the defined geometry.

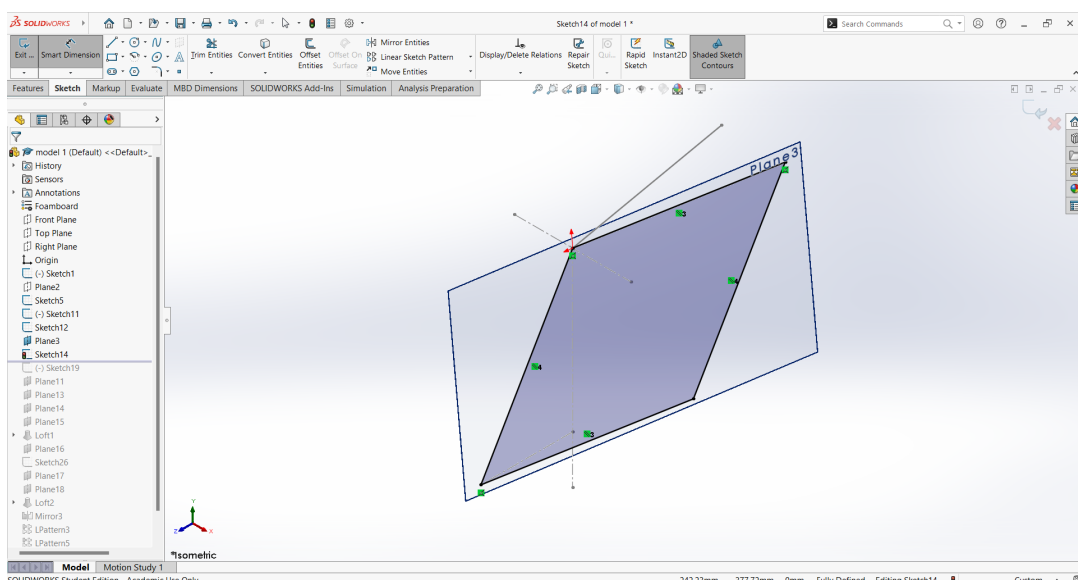


Figure 4.5: Sketching the first parallelogram panel

Another sketch was then created on the right plane using the ‘Line’ construction tool, that mirrors the left edge of the parallelogram. The ‘Smart Dimension’ tool was used to check that this new line is also 200mm:

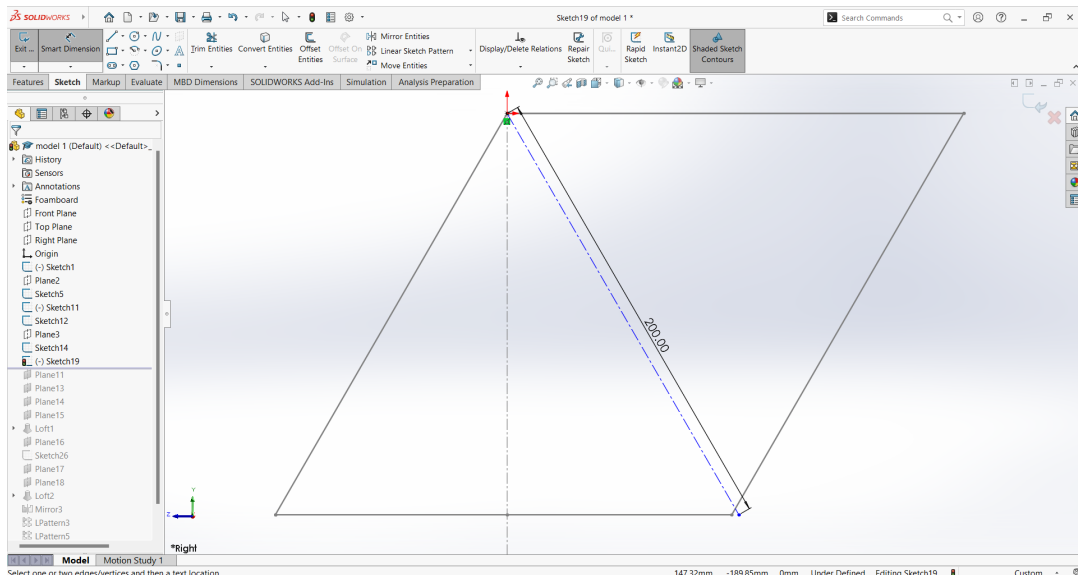


Figure 4.6: Creating a construction line for reference

Another reference plane was created in a similar way as in Figure 4.4, with the selected lines pictured in Figure 4.7.

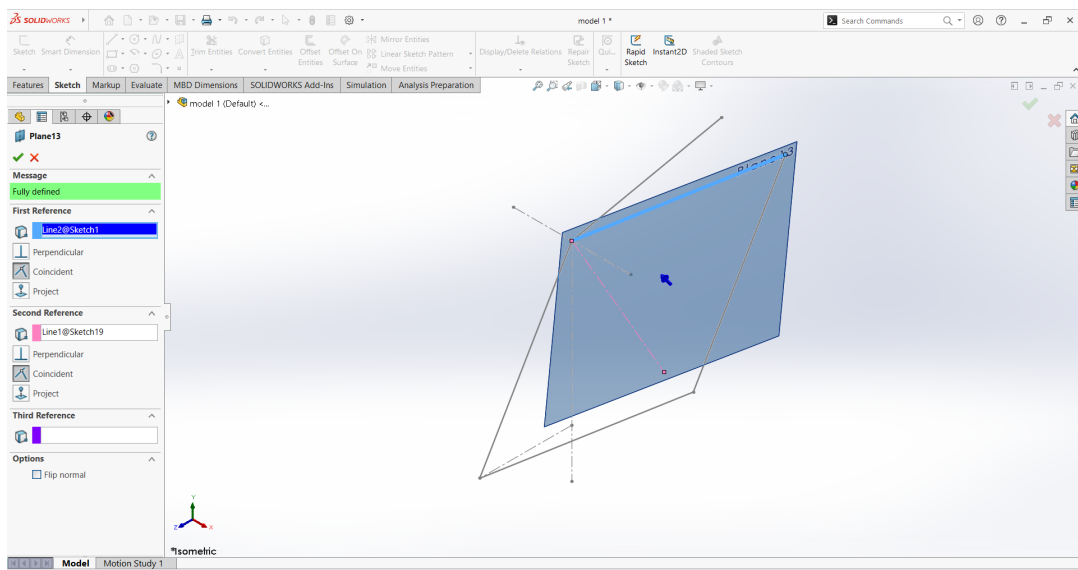


Figure 4.7: Creating the second reference plane

In the same was as in Figure 4.5, a new sketch was created on this new reference plane. The same parallelogram with identical dimensions was sketched, with the only difference being that the second parallelogram is slanted such that the first parallelogram seems to have been reflected in the front plane. This can be seen in Figure 4.8:

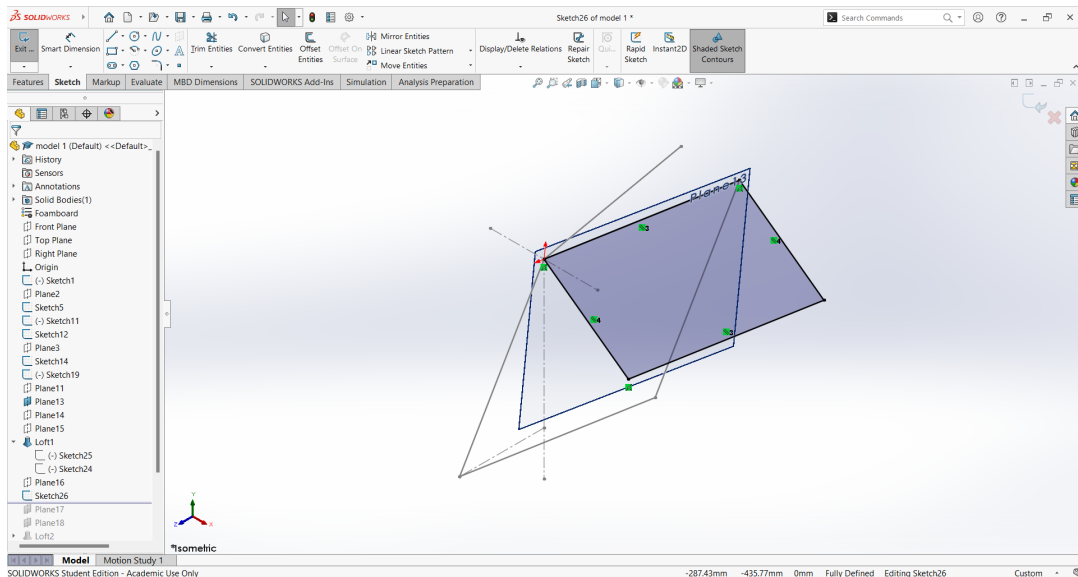


Figure 4.8: Sketching the second parallelogram panel

Three more reference planes were created, one for the top edge and one for the bottom edge of both parallelograms (the top edges coincide, therefore one plane is sufficient), as shown in Figure 4.9:

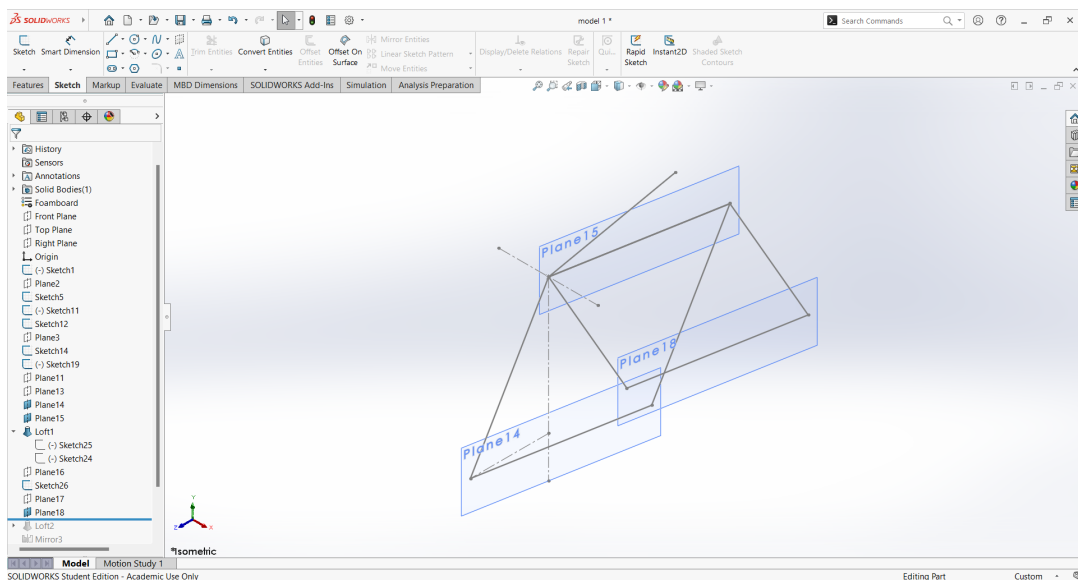


Figure 4.9: Creating three reference planes for thickness sketches

Starting with the top most plane, a rectangle of length 200mm and width 3mm was sketched using the ‘Rectangle’ tool, pictured in Figure 4.10, with one edge coincident with the parallelogram edge. The width value corresponds to a material thickness of 3mm, which was chosen to allow the replication of these models in real life using the accessible foamboard in the university laboratory that has that same thickness.

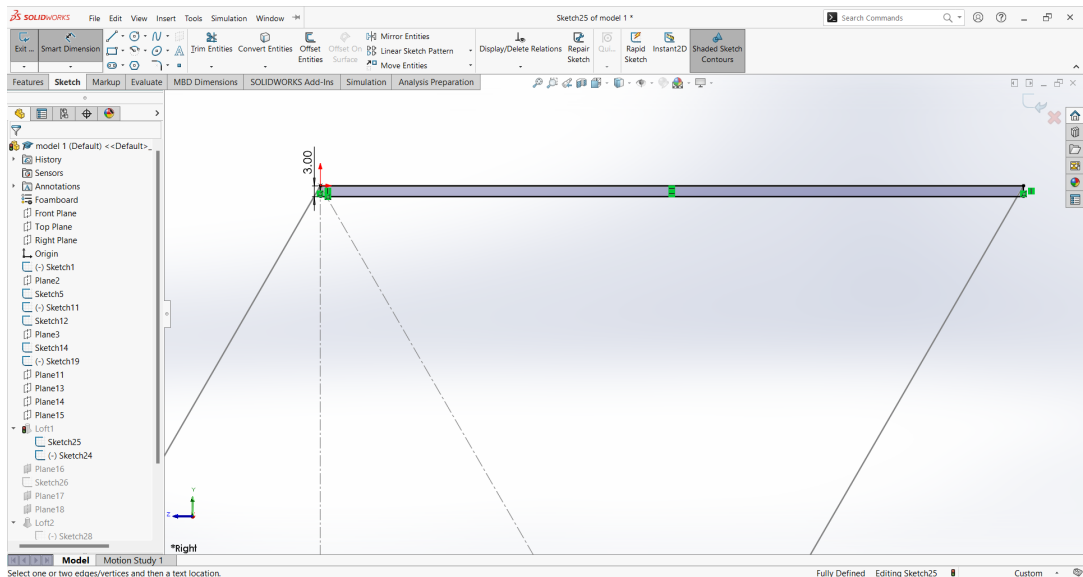


Figure 4.10: Sketching the cross section of the panel

The steps taken in Figure 4.10 were repeated for each plane shown in Figure 4.9, producing a model as shown in Figure 4.11 in isometric view:

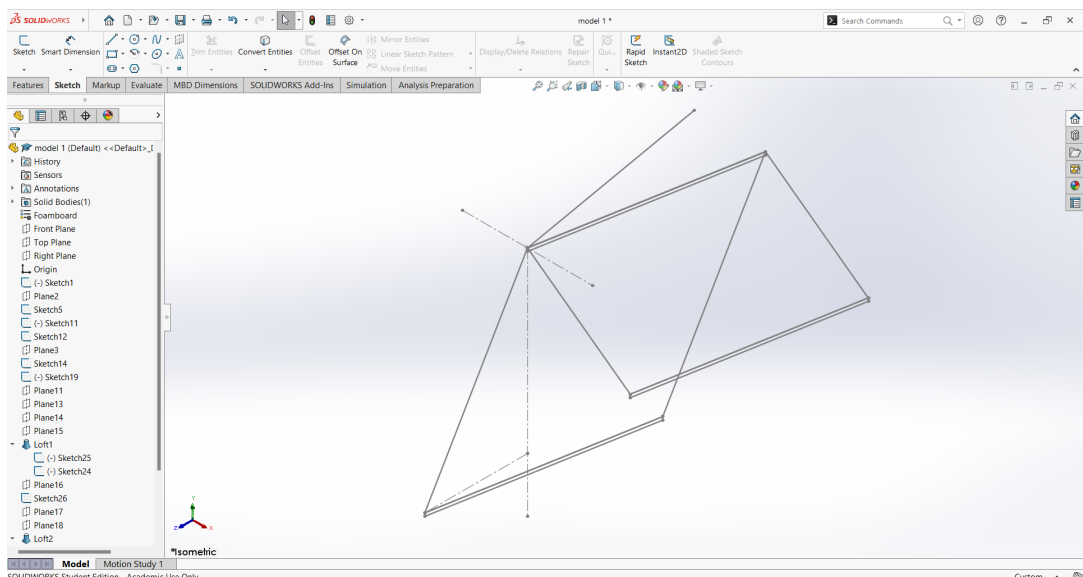


Figure 4.11: All thickness sketches created

In the ‘Features’ section of the ‘Command Window’, the ‘Lofted Boss/Base’ feature was selected. The two sketches (rectangles created as in Figure 4.10) shown in Figure 4.11 were selected as the profiles to create the loft. This step gives the model its thickness and creates one complete panel out of the four required for a Miura unit cell:

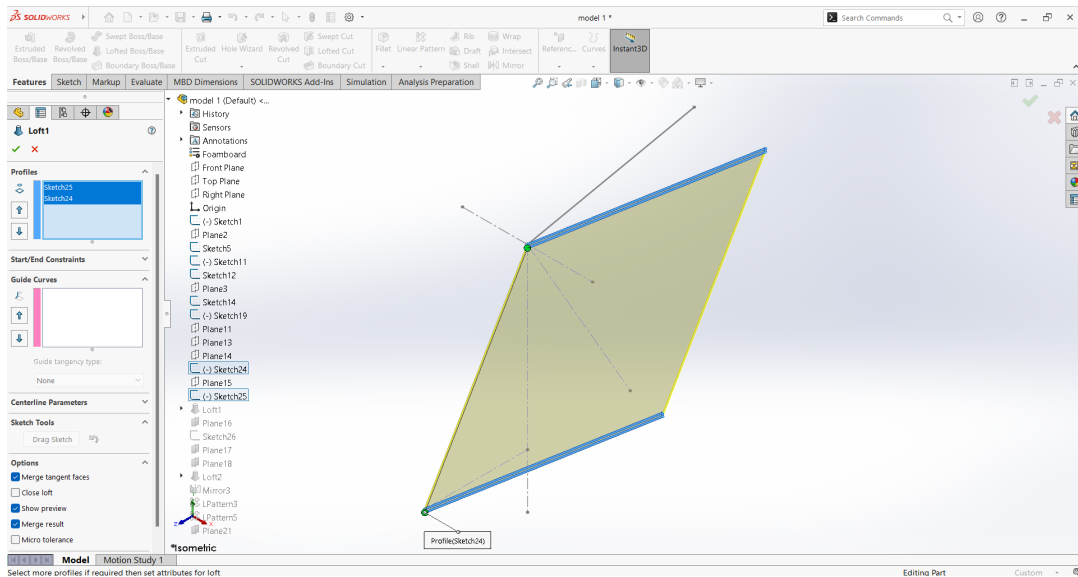


Figure 4.12: Creating a loft to produce a solid body

This step was repeated for the rectangular sketches that correspond to the second parallelogram created as shown in Figure 4.8 and the lofted model at this stage (half of a Miura unit cell) is shown in Figure 4.13.

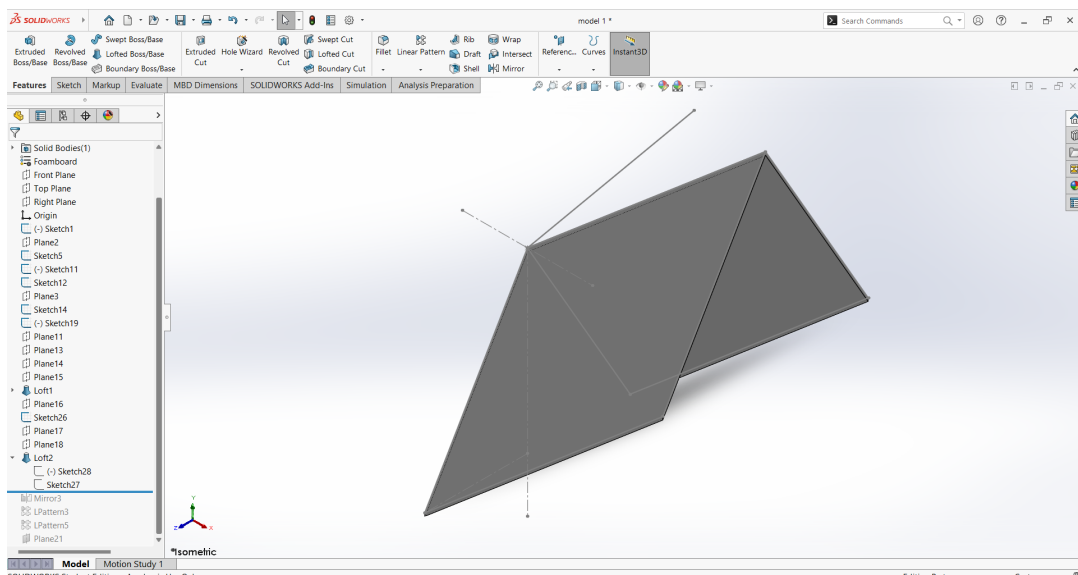


Figure 4.13: Creating the second loft

Next, the model was reflected in the right plane using the ‘Mirror’ feature. Figure 4.14 highlights that the entire body created in Figure 4.13 was mirrored in the right plane and the option to ‘Merge Solids’ was ticked. This ensures that the panels combine to simulate a monolithic model, rather than acting as separate structures that have been glued together.

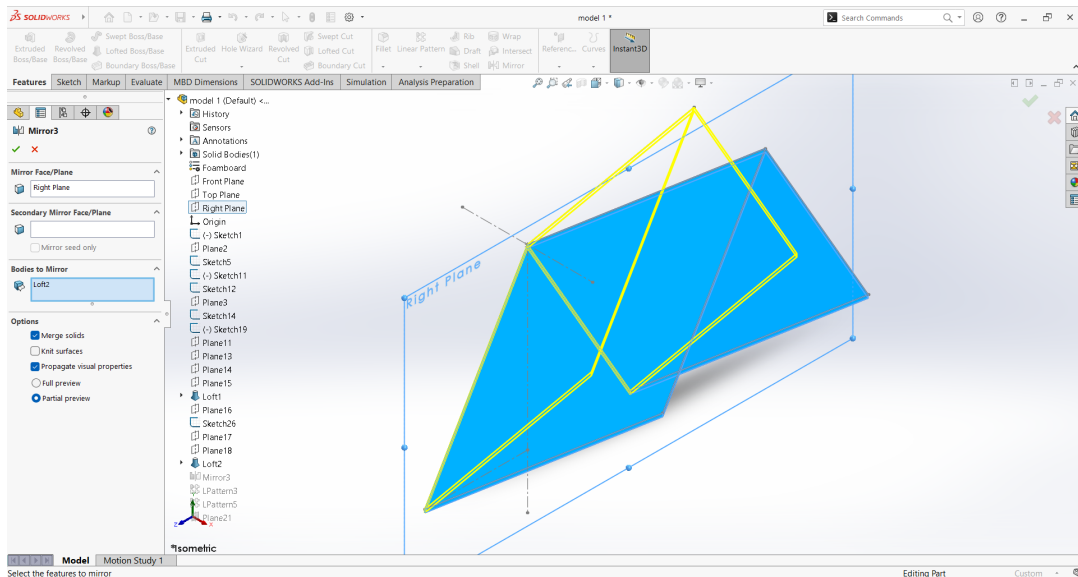


Figure 4.14: Mirroring the model to create one Miura unit cell

At this stage, one complete Miura unit cell has been created and this can simply be copied rather than redoing the method until this point. Figure 4.15 shows the use of the ‘Linear Pattern’ feature, resulting in the unit cell being copied three more times. Key details to note are that the entire body of the original unit cell was selected and they are 69.46mm apart to ensure that each new body touches the previous one without any overlap.

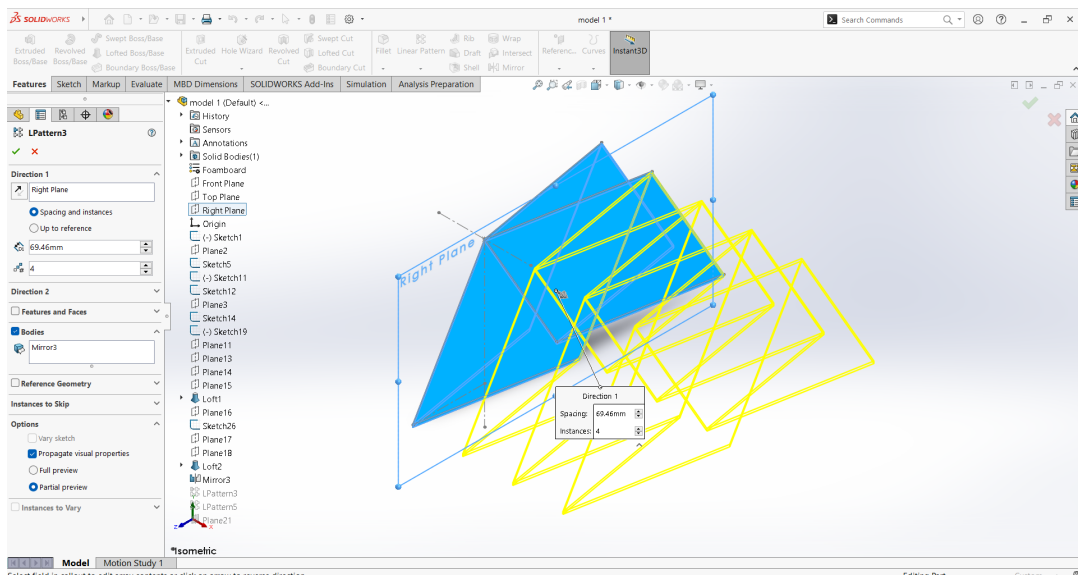


Figure 4.15: Linear patterning the Miura unit cell in the right plane

In the final step for model creation, the ‘Linear Pattern’ feature was used again, this time patterning in the front plane direction, as pictured in Figure 4.16. The final output of the first model is shown in Figure 4.17, which is a Miura folded pattern

comprising of 16 unit cells with a thickness of 3mm.

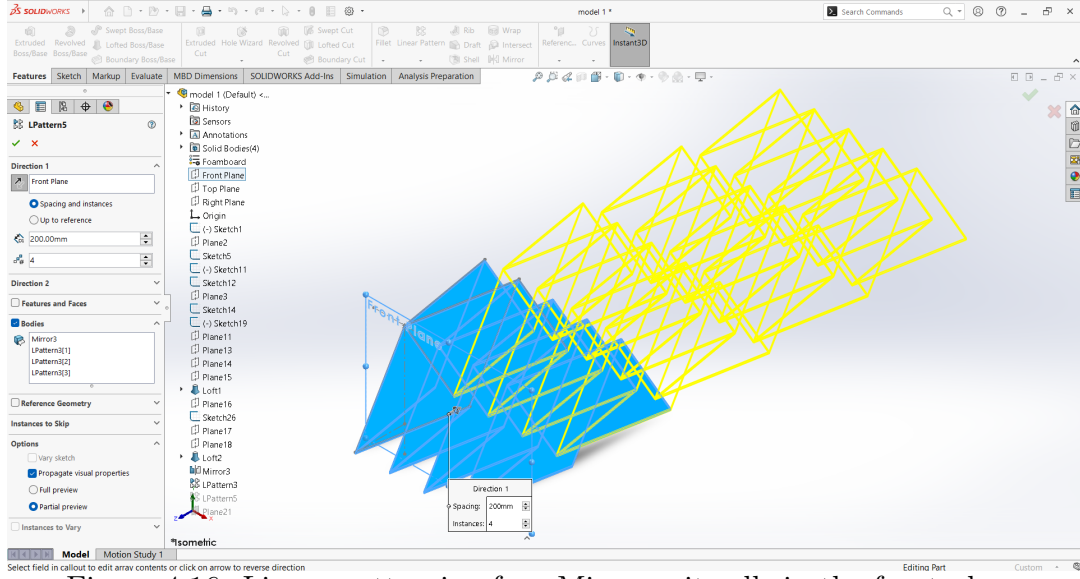


Figure 4.16: Linear patterning four Miura unit cells in the front plane

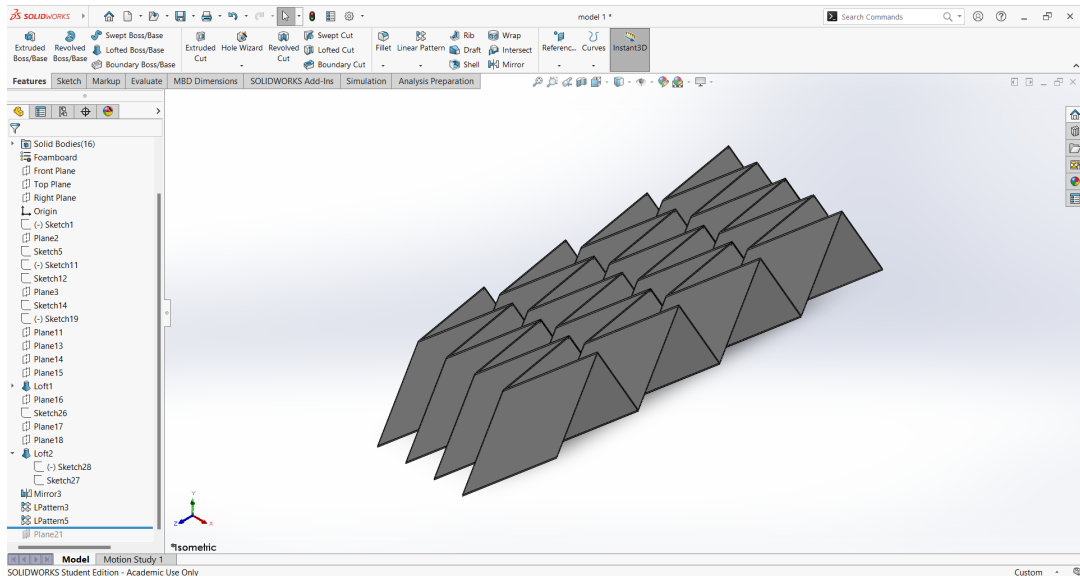


Figure 4.17: Final result for model 1

In order to create the first five models, the method until this point was repeated and each time, the side length of the parallelograms, a , (set in Figures 4.5 and 4.8, respectively) were altered to achieve five distinct ratios for the panel dimensions. In this way, five models with different tessellation patterns were created, each with a thickness of 3mm. The value b was kept constant at 200mm and a was changed to achieve the desired $b : a$ ratios, shown in Table 4.1:

Model number	b:a ratio	a (mm)	H (mm)
1	1:1	200.00	173.21
2	1:2	400.00	348.15
3	1:1.5	300.00	261.11
4	2:1	100.00	86.60
5	1.5:1	133.33	115.47

Table 4.1: Chosen geometry ratios and their corresponding parallelogram side lengths (a) and model heights (H)

These ratios were chosen in order to gain and understanding of the implications of a wide range of Miura patterns. Equations (3.9) and (3.11) depend solely on these values (see Figure 3.5): $b = 200\text{mm}$, $\gamma = 60.5$ and $\theta = 84.27$. Since these were all set as control variables, S and V also remained the same for all five models. These values were found to be 69.46mm and 196.96mm respectively, using the ‘Smart Dimension’ tool in Solidworks. This tool was also used to find the value of θ , considering fold angle $= 2\xi = 20^\circ$. Models with fold angles of less than 20° were not possible to create on Solidworks once model thickness was taken into consideration. Given that a was a value that was set in Solidworks, the $2L$ values, found from equation (3.10) were exactly equal to the a values for each model.

4.2.2 Creating FEA simulations

Once the first five models were created, a static study was also established for each one in order to allow the visualisation of the stresses, strains and displacement of each model. For example, this was done for model 1 as follows:

In the Solidworks ‘Command Window’ under ‘Simulation’, a new study was created and under ‘General Simulation’, ‘Static Study’ was selected, with the ‘2D Simplification’ box unticked. From the ‘Fixtures’ tab, ‘Fixed Geometry’ was selected and the four faces shown in Figure 4.18 were selected:

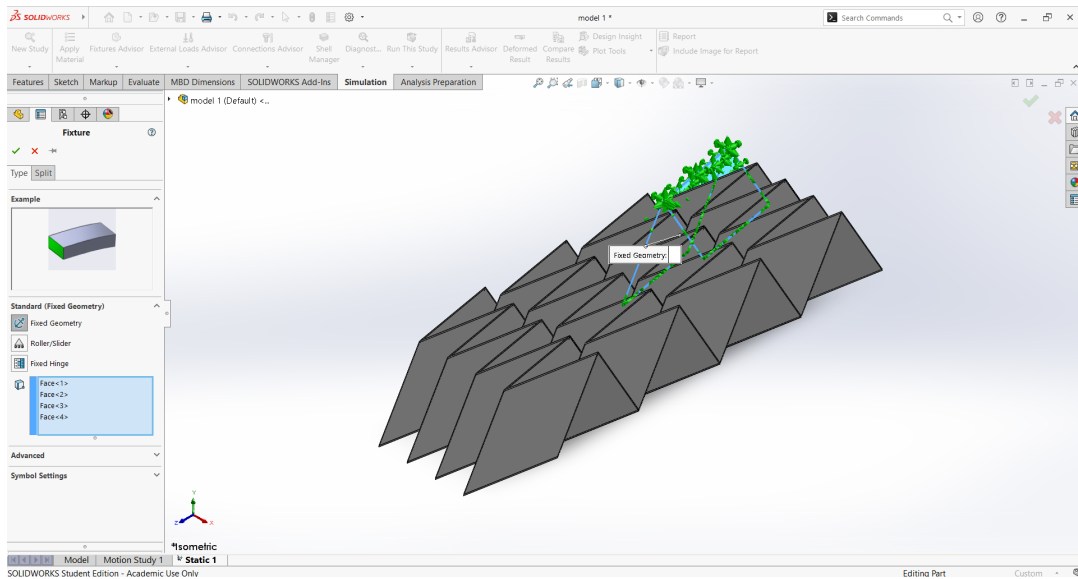


Figure 4.18: Setting fixture panels

Then, from the external load advisor, ‘Force’ was selected. The back of the panels shown in Figure 4.19 were selected in order to more accurately simulate deployment force, at 10N per panel.

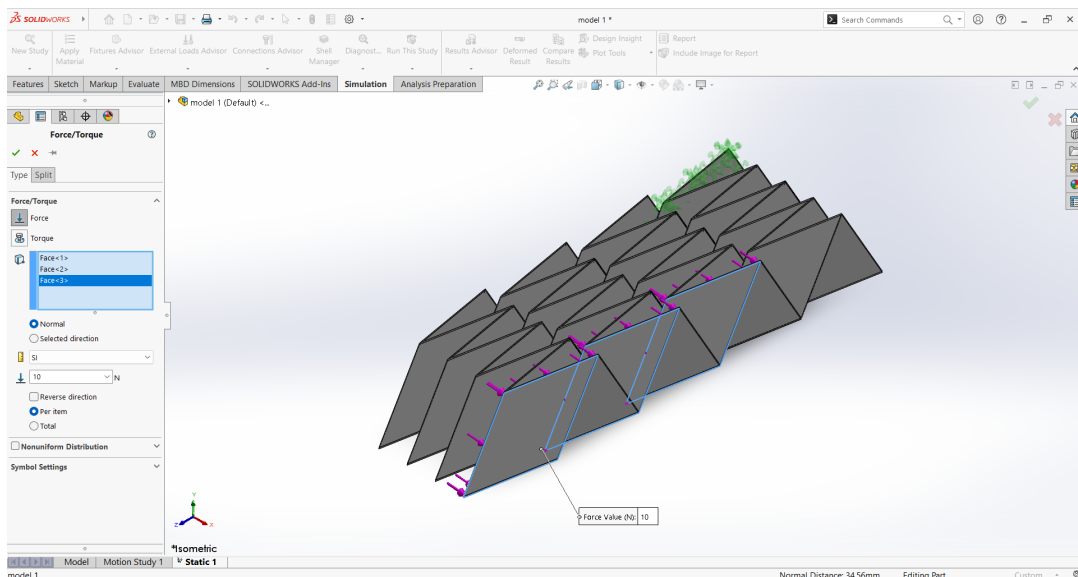


Figure 4.19: Setting the force applied on the panels

Finally, before running the simulation, a mesh was created. The ‘Blended Curvature Based Mesh’ was selected to ensure the solution could be solved accurately, even near sharp edges. Other than the minimum number of elements in a circle (shown to be 32 in Figure 4.20), all default settings were used:

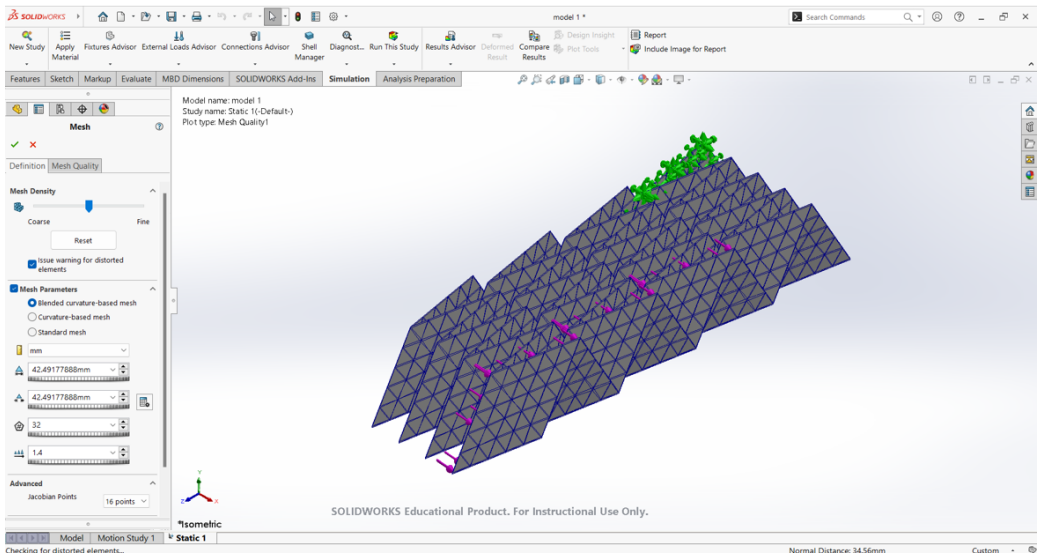


Figure 4.20: Creating the mesh

These steps were repeated for all five models and each study was then run to obtain results for stress, displacement and strain.

4.2.3 Changing the material

The final parameter to change is the material. Once the first ten models had been created and simulations had been run to obtain results, it was possible to compare these results to determine which model provided the most feasible solution for a foamboard horn antenna panel prototype. This material was automatically set in the ‘Feature Manager Design Tree, as its material properties were already saved in the Solidworks material database.

The final four models were created using the same physical model as model 6. This was to ensure the $b : a$ ratio was 1:1 and that the thickness was 1mm, as the suitable materials being tested are the ones detailed in section 3.2. In order to obtain results that would allow the comparison of stress, displacement and strain between different materials, thickness must be kept the same. 1mm was chosen because this was the most common thickness of which Nitinol, PEEK, Kapton and CFRP can be manufactured on a large scale. A greater thickness than this would make the Kapton model results invalid and a lower thickness would make the CFRP and PEEK model results invalid because relatively, they are manufactured with lower and higher thicknesses, respectively. A 1mm thickness throughout models 11 to 14 provided the

best overlap for feasible collection and comparison of results.

In the ‘Feature Manager Design Tree’, ‘Edit Material’ was selected, followed by ‘New Material’. The material property values required were inputted and applied to the relevant model (shown in Figure 4.21) for each material.

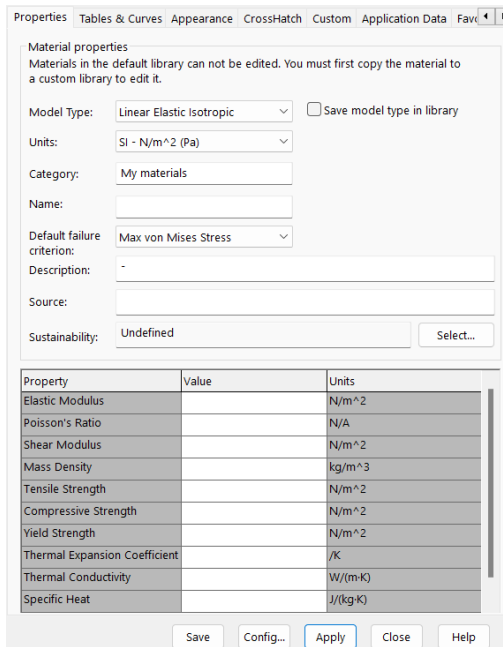


Figure 4.21: Defining the material properties

Upon completion of this methodology, the following models and simulations were created and run:

- **Models 1-5:** 3mm thick foamboard models with $b : a$ ratios of 1:1, 1:2, 1:1.5, 2:1 and 1.5:1, respectively. Stress, displacement and strain plots with results legends produced for each.
- **Models 6-10:** foamboard models with a $b : a$ ratio of 1:1 and thicknesses of 1mm, 2mm, 5mm, 10mm and 20mm, respectively. Stress, displacement and strain plots with results legends produced for each.
- **Models 11-14:** 1mm thick models with a $b : a$ ratio of 1:1 and materials Nitinol, PEEK, Kapton and CFRP, respectively. Stress, displacement and strain plots with results legends produced for each.

5 Results

This section shows all 14 models created in their fully folded state, with three plots for each one, showing stress, strain and displacement.

5.1 Varying b:a ratio

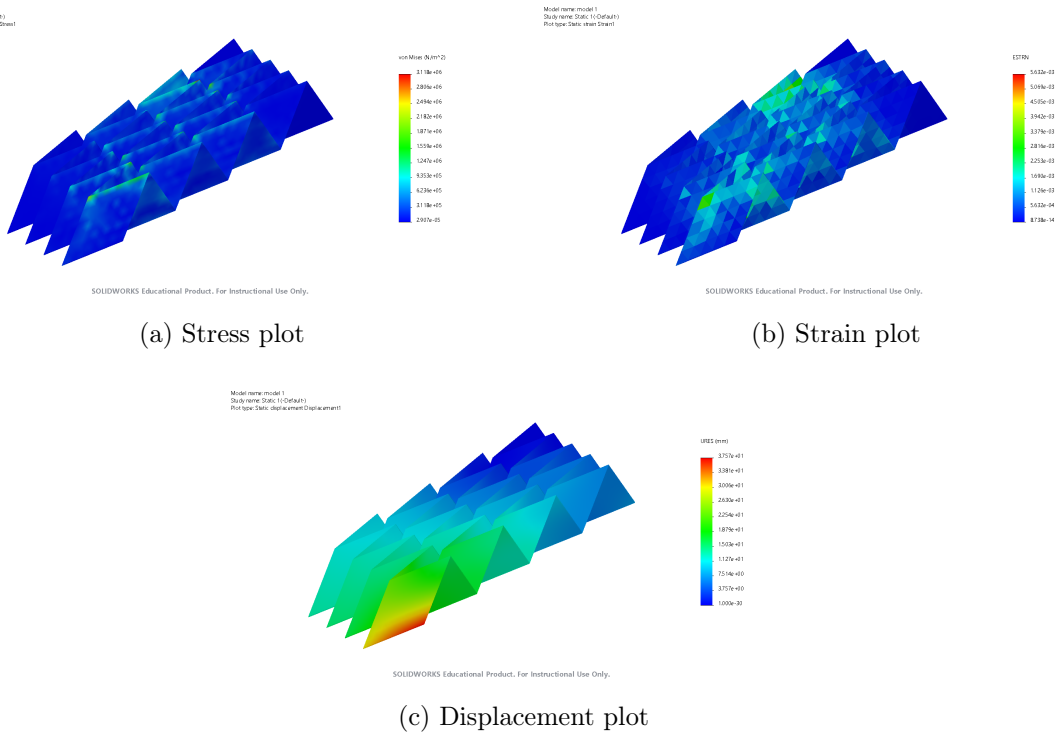


Figure 5.1: Model 1 results: 3mm thick foamboard and 1:1 ratio

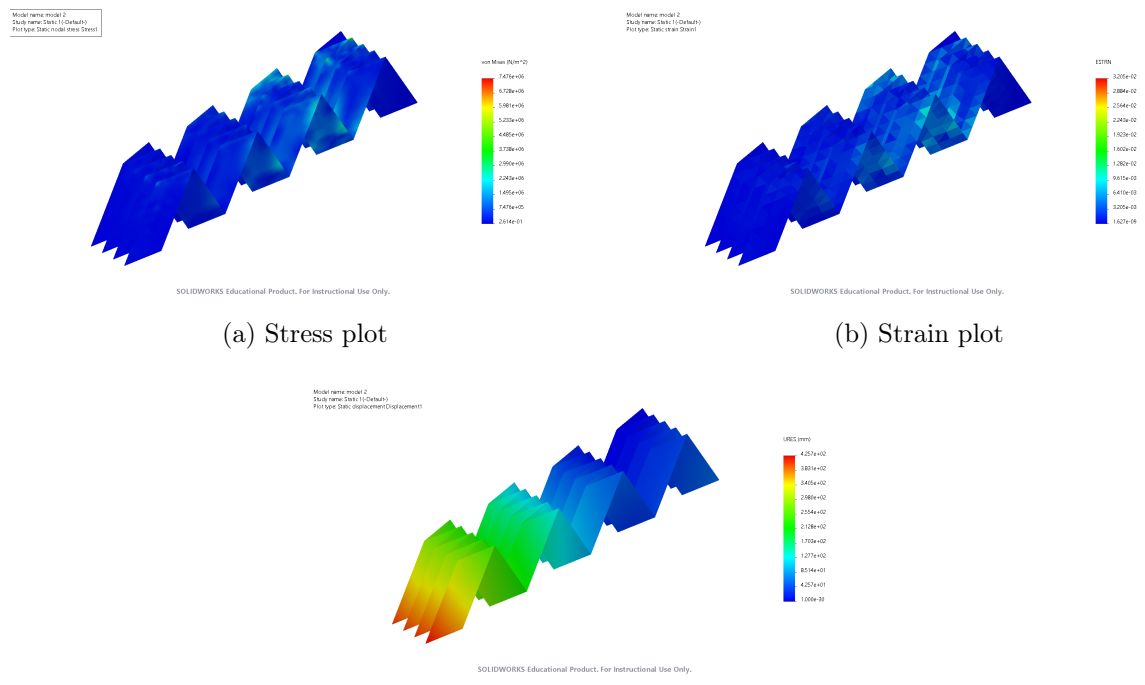
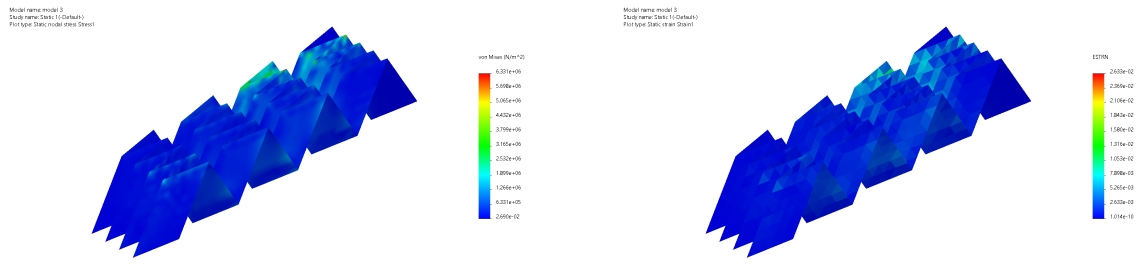
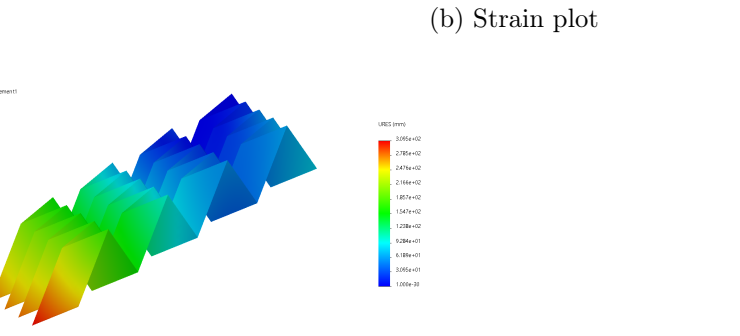


Figure 5.2: Model 2 results: 3mm thick foamboard and 1:2 ratio

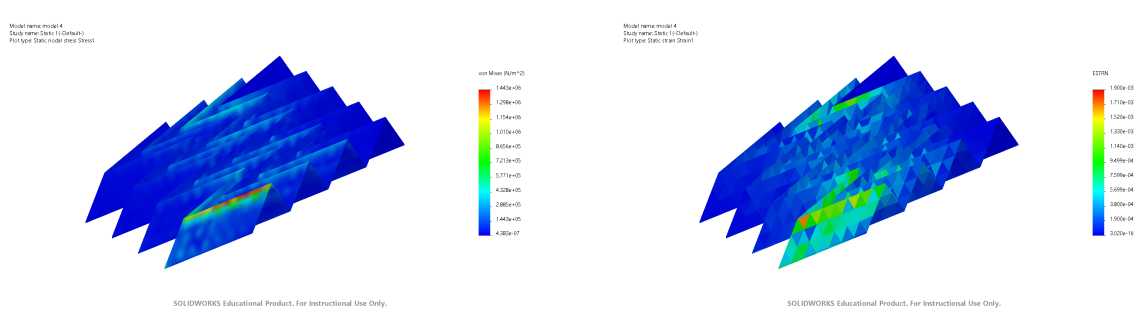


SOLIDWORKS Educational Product, For Instructional Use Only.

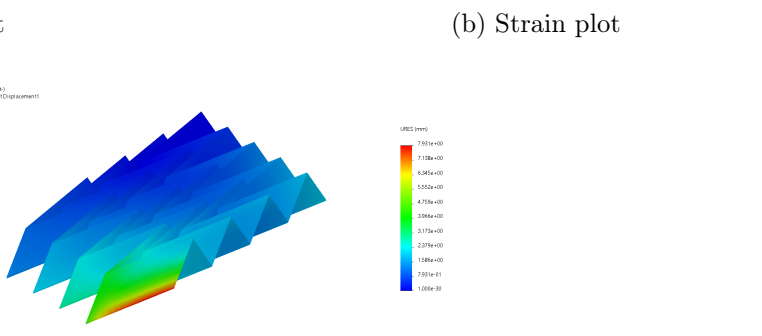


SOLIDWORKS Educational Product, For Instructional Use Only.

Figure 5.3: Model 3 results: 3mm thick foamboard and 1:1.5 ratio



SOLIDWORKS Educational Product, For Instructional Use Only.



SOLIDWORKS Educational Product, For Instructional Use Only.

Figure 5.4: Model 4 results: 3mm thick foamboard and 2:1 ratio

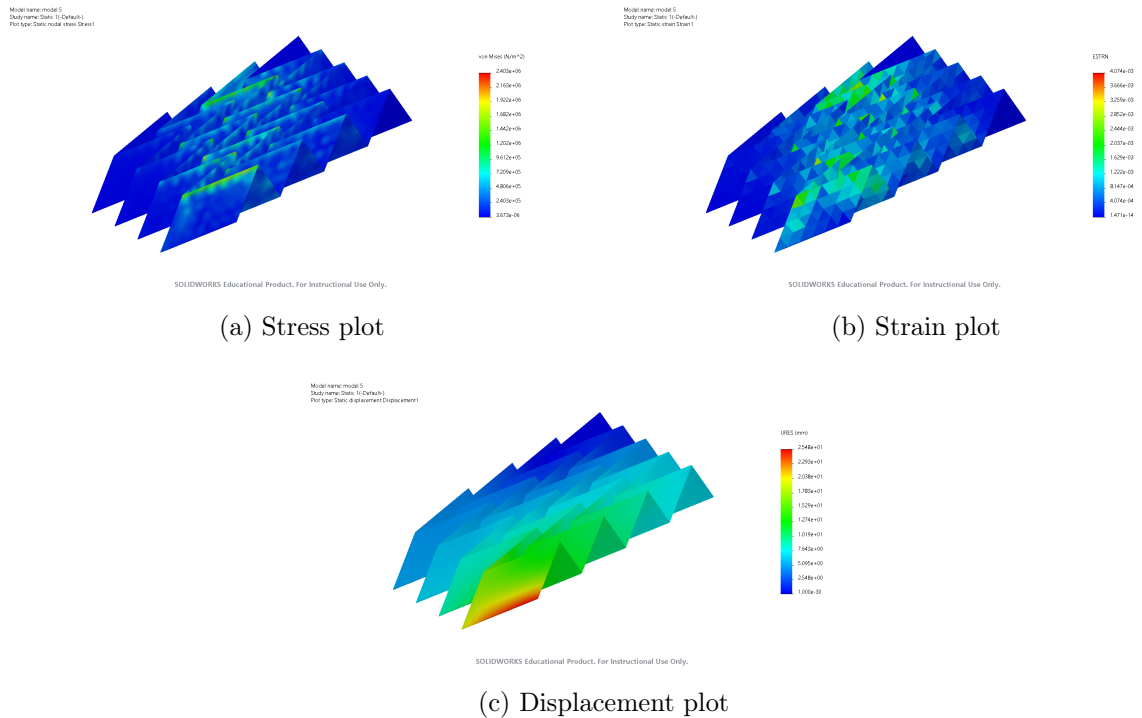


Figure 5.5: Model 5 results: 3mm thick foamboard and 1.5:1 ratio

The results produced from these five models provide a basis on which to test objectives 1 and 2.

5.2 Varying thickness

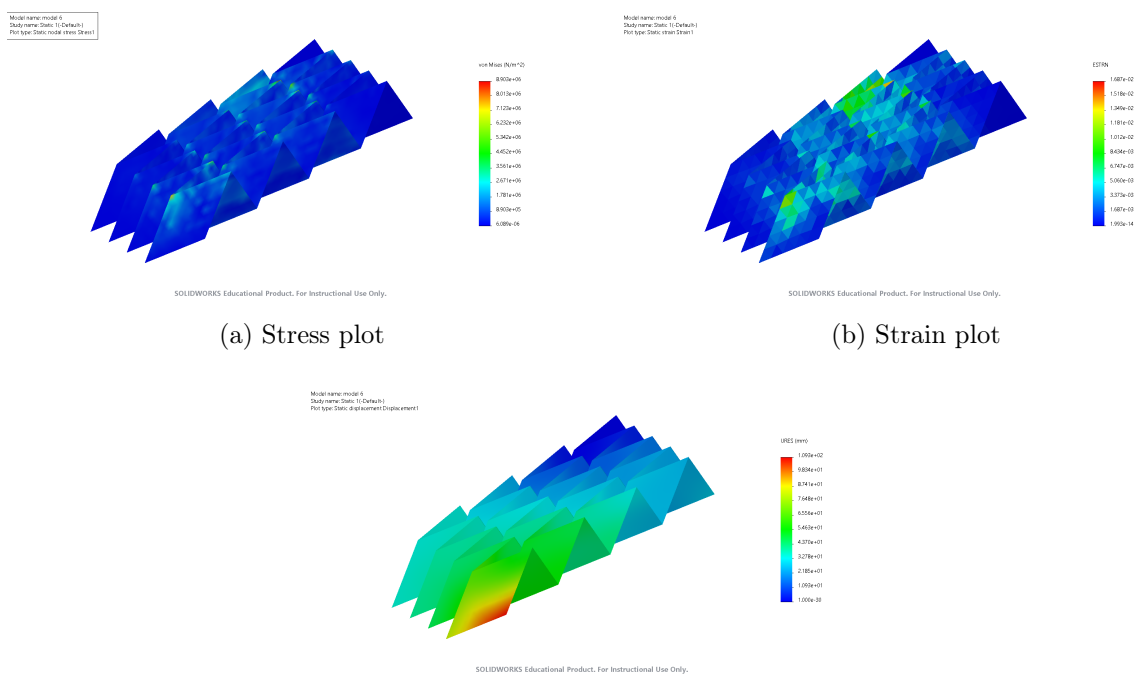


Figure 5.6: Model 6 results: 1mm thick foamboard and 1:1 ratio

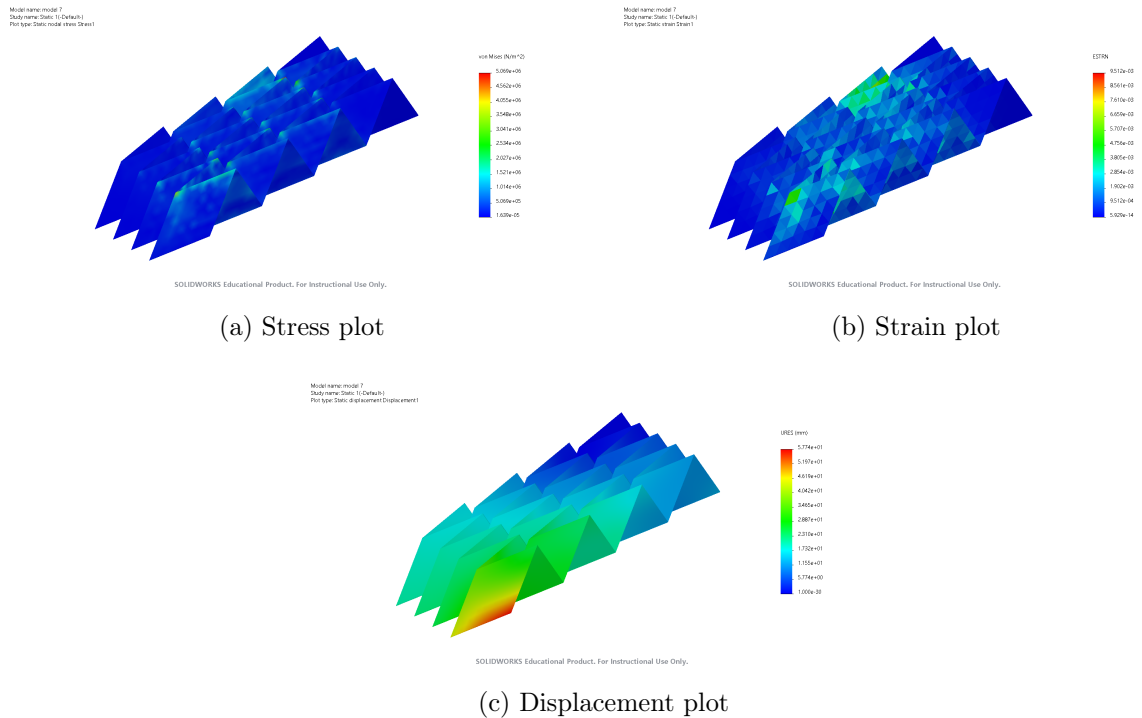


Figure 5.7: Model 7 results: 2mm thick foamboard and 1:1 ratio

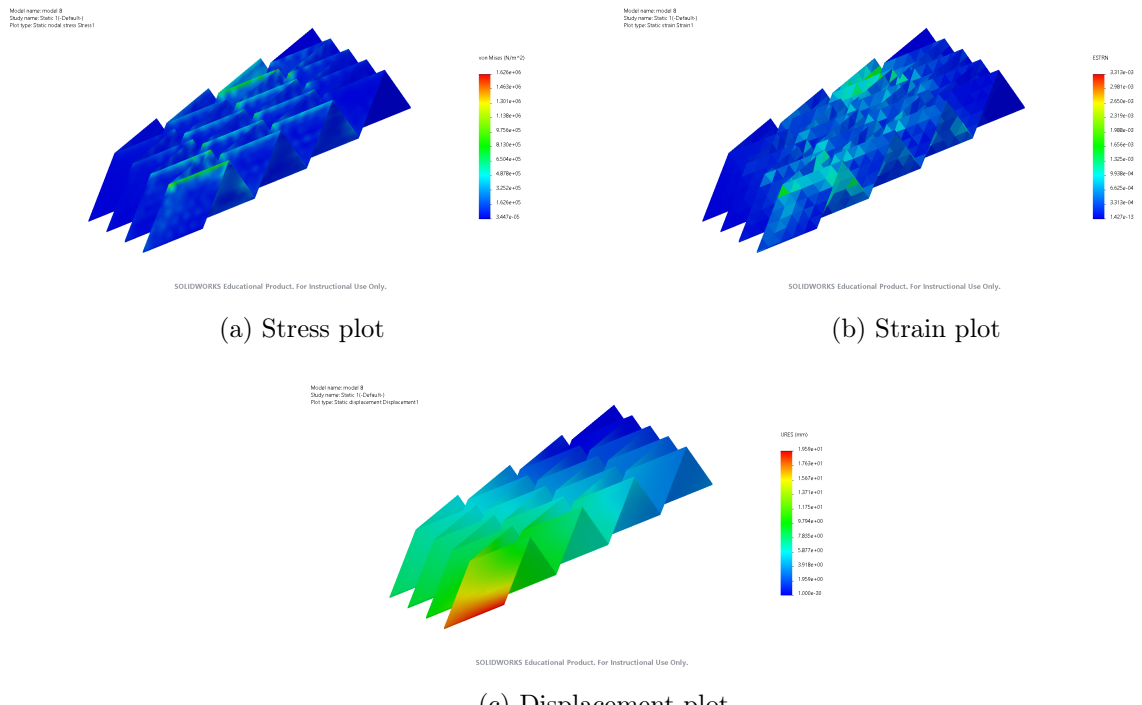
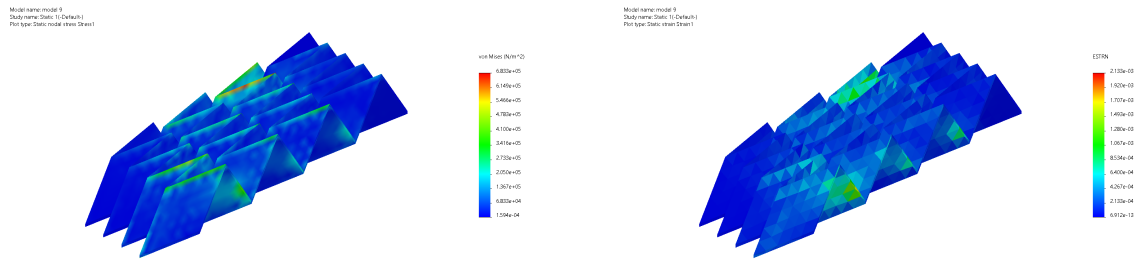
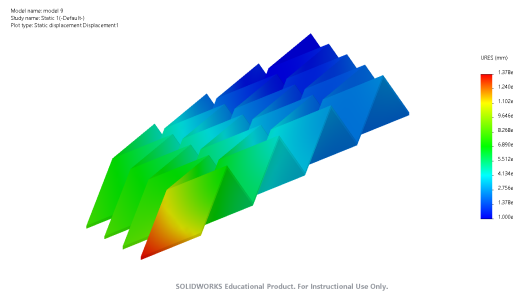


Figure 5.8: Model 8 results: 5mm thick foamboard and 1:1 ratio



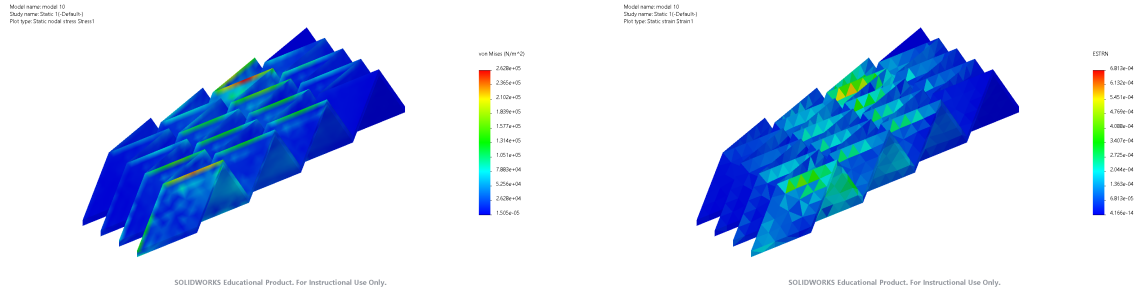
(a) Stress plot

(b) Strain plot



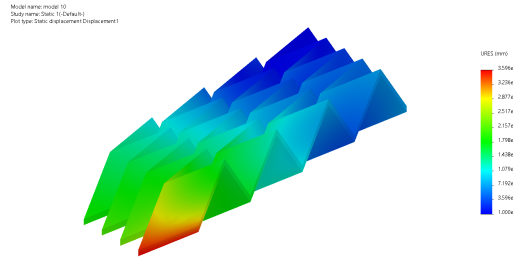
(c) Displacement plot

Figure 5.9: Model 9 results: 10mm thick foamboard and 1:1 ratio



(a) Stress plot

(b) Strain plot



(c) Displacement plot

Figure 5.10: Model 10 results: 20mm thick foamboard and 1:1 ratio

The results produced from these five models provide a basis on which to test objectives 1 and 2.

5.3 Varying material

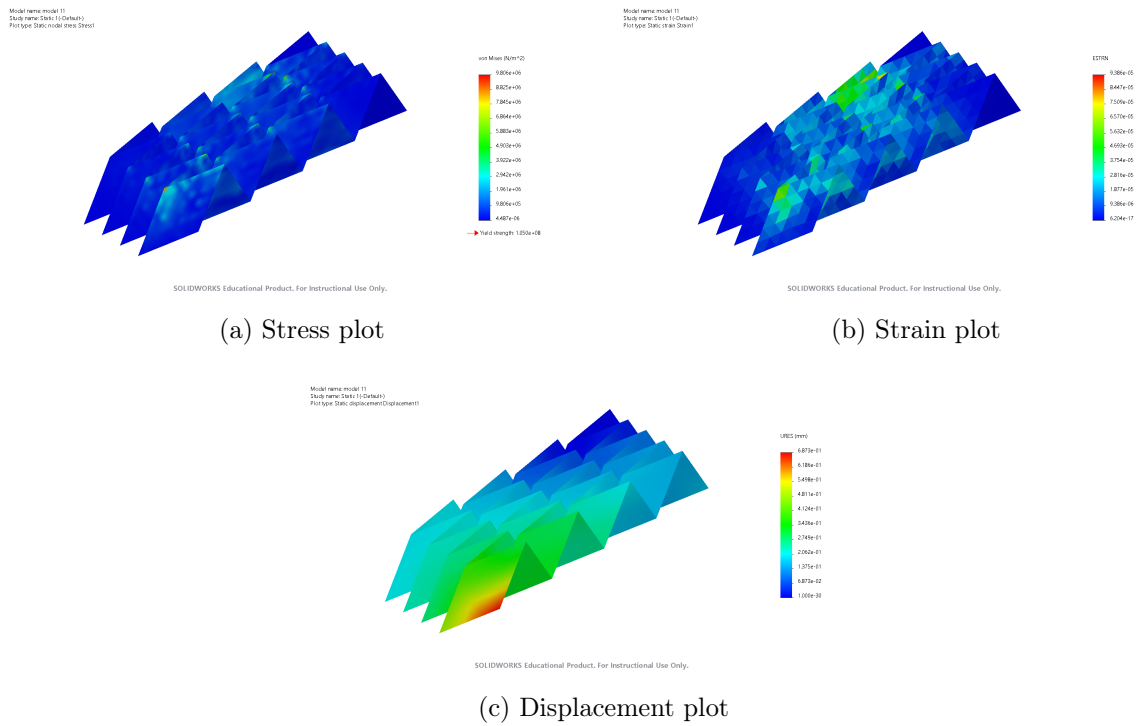


Figure 5.11: Model 11 results: 1mm thick Nitinol and 1:1 ratio

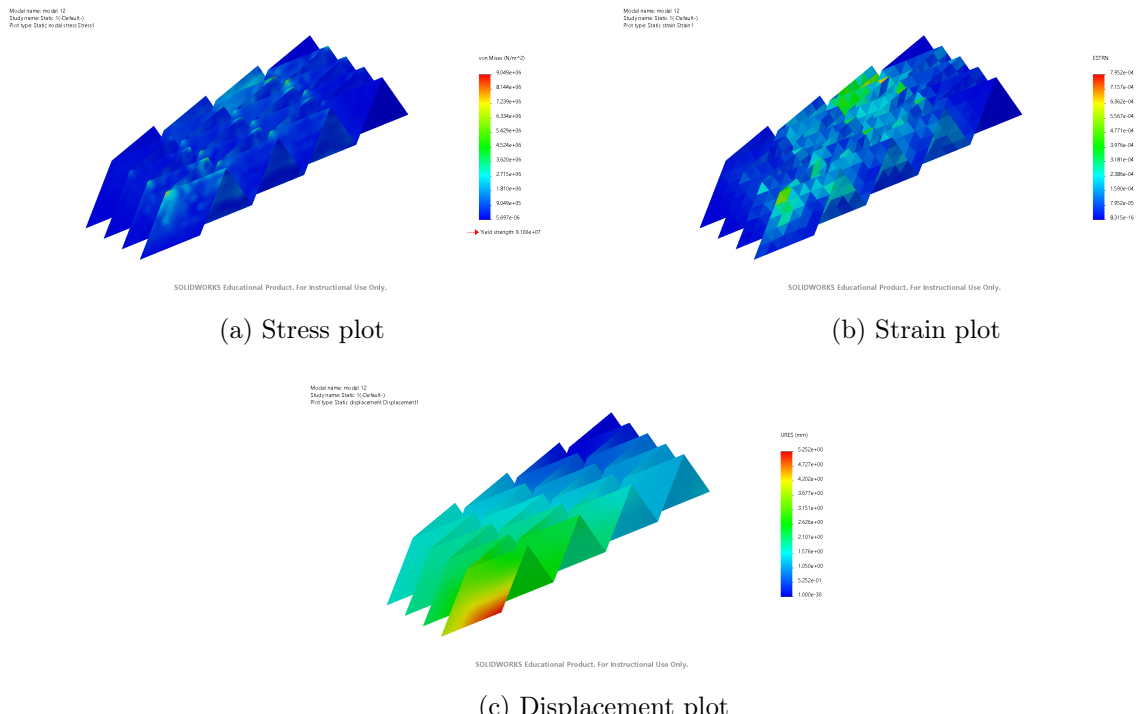
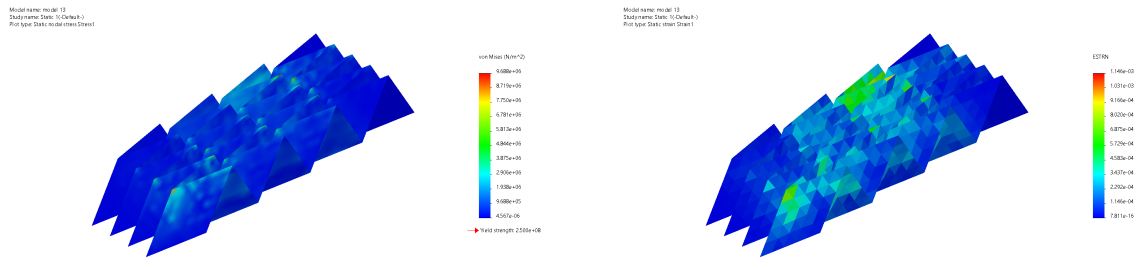


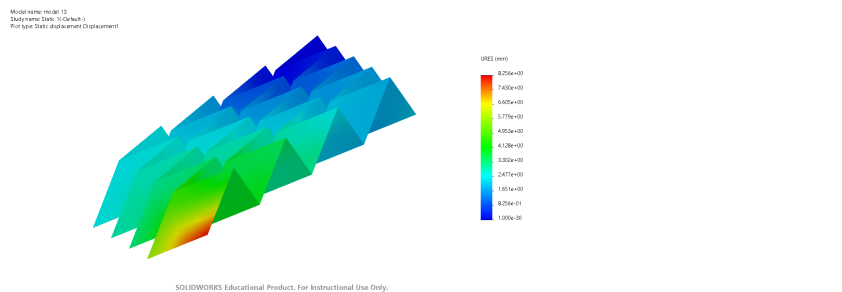
Figure 5.12: Model 12 results: 1mm thick PEEK and 1:1 ratio



(a) Stress plot

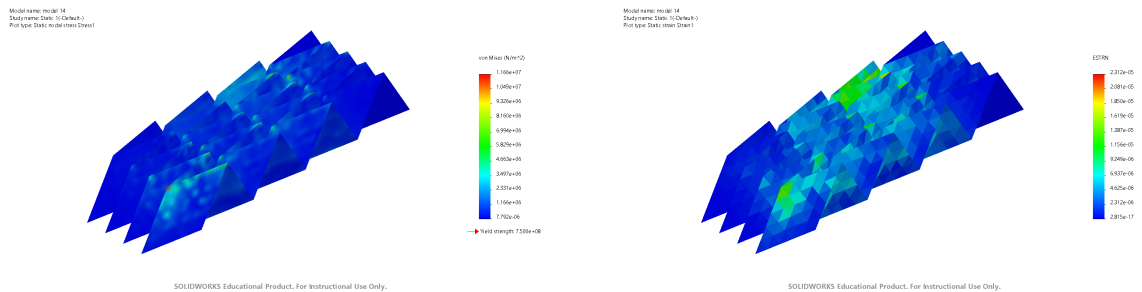
SOLIDWORKS Educational Product, For Instructional Use Only.

(b) Strain plot



(c) Displacement plot

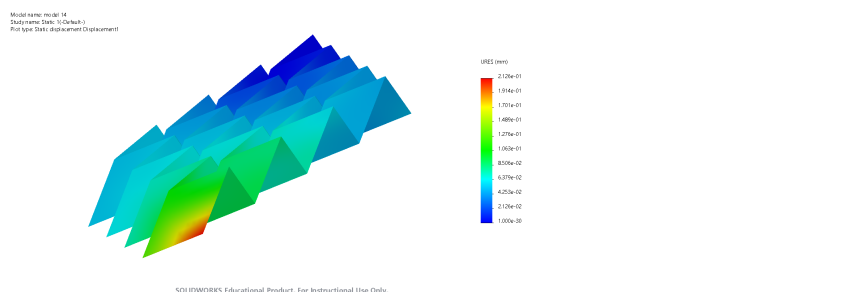
Figure 5.13: Model 13 results: 1mm thick Kapton and 1:1 ratio



(a) Stress plot

SOLIDWORKS Educational Product, For Instructional Use Only.

(b) Strain plot



(c) Displacement plot

Figure 5.14: Model 14 results: 1mm thick CFRP and 1:1 ratio

The results produced from these four models provide a basis on which to test objectives 1, 2 and 3.

Material Property	Units	Material			
		Nitinol	PEEK	Kapton	CFRP
Elastic Modulus	N/m^2	3.450×10^{10}	3.855×10^9	2.760×10^9	1.300×10^{11}
Poisson's Ratio	-	0.3300	0.3855	0.3400	0.1000
Shear Modulus	N/m^2	1.295×10^{10}	1.391×10^9	2.750×10^9	5.000×10^9
Mass Density	kg/m^3	6450	1310	1430	1600
Tensile Strength	N/m^2	1.900×10^9	8.665×10^7	1.850×10^8	6.000×10^8
Compressive Strength	N/m^2	1.50×10^9	1.24×10^8	2.75×10^8	5.70×10^8
Yield Strength	N/m^2	1.05×10^8	9.10×10^7	2.50×10^8	7.50×10^8
Thermal Expansion Coefficient	/K	6.600×10^{-6}	1.332×10^{-4}	2.000×10^{-5}	2.100×10^{-6}
Thermal Conductivity	$W/(mK)$	8.60	0.25	0.12	12.50
Specific Heat	$J/(kgK)$	837	1386	1090	1100

Table 5.1: Material properties for Nitinol (Alipour et al. 2022), PEEK (Skirbutis et al. 2018), Kapton (Alarcón López 2017) and CFRP (Kumar, R. Singh, and Sharma 2021)

Table 5.1 shows the material properties that were inputted into Solidworks (see Figure 4.21) and average values were used when ranges were given.

5.4 Uncertainty analysis

5.4.1 Mesh element size

Obtaining reliable results requires a certain element size to be set. When creating the mesh, detailed in section 4.2.2, the value used for both maximum and minimum element size was 42.49177888mm, which created a uniform mesh. This value was decided using a mesh convergence technique, by collecting maximum stress values for model 1 at different mesh sizes. Starting with the coarsest mesh possible, mesh size was reduced until the value of maximum stress converged to a value which resulted in a sensitivity index with a magnitude of less than 2%.

Figure 5.15 shows a plot of this convergence and the trend in sensitivity index can be seen in Table 5.2. Since this value converged to a less than 2% difference, the value used for element size in the methodology can be considered as reliable and the uncertainty produced in the results by the mesh size is relatively negligible due to the mesh refinement process.

Element Size (mm)	Maximum Stress N/m^2	Sensitivity Index (%)
64.99177888	1056308.088	6.062161535
62.49177888	995933.0198	-78.90372601
59.99177888	4720895.36	81.68513707
57.49177888	2598393.813	-18.00287228
54.99177888	3168883.941	10.29612657
52.49177888	2873069.109	-8.09667489
49.99177888	3126186.246	4.624026428
47.49177888	2988019.438	-2.989900522
44.99177888	3080111.714	-1.208897388
42.49177888	3117802.75	-

Table 5.2: Mesh element size used for models and their corresponding maximum stress values and calculated sensitivity index

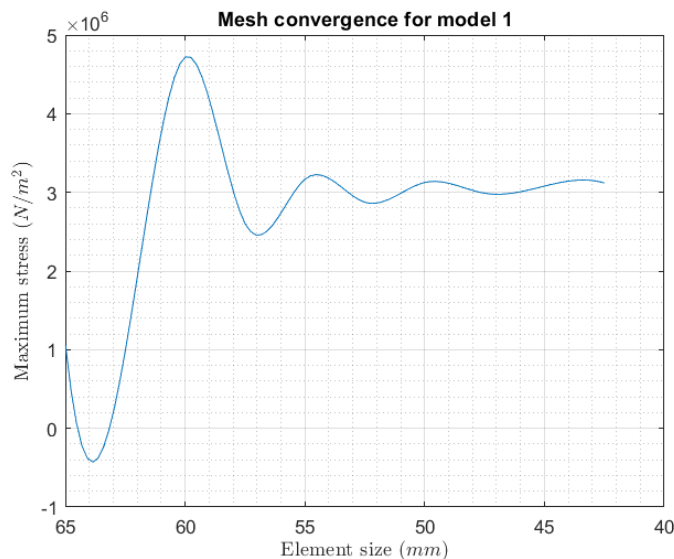


Figure 5.15: Mesh convergence as a result of mesh refinement

The initial element size in Table 5.2 corresponds to the coarsest mesh that can produce valid results and is an exact value, as it is calculated by the software. Increments of 2.5mm were taken to refine the mesh slowly and after nine iterations, the mesh converged. The final value for element size was then used for all models when running simulations.

5.4.2 Material properties

The percentage uncertainty in each material (detailed in Table 5.3) used for this analysis is based on relevant literature (Gabauer 2000).

Material	Material Property	Uncertainty Value	Maximum Stress (N/m^2)	Sensitivity Index (%)
Nitinol	Elastic modulus (N/m^2)	$+2\% = 3.519 \times 10^{10}$	9805700	-0.004589163
		$-2\% = 3.381 \times 10^{10}$	9805709	0
	Poisson's Ratio (-)	$+2\% = 0.3366$	9728504	0.787347452
		$-2\% = 0.3234$	9880373	-0.761433977
PEEK	Elastic modulus (N/m^2)	$+2\% = 3.9321 \times 10^9$	9048766	0.001105123
		$-2\% = 3.7779 \times 10^9$	9048780	-0.008840986
	Poisson's Ratio (-)	$+2\% = 0.39321$	8917424	1.451468952
		$-2\% = 0.37779$	9171940	-1.361246685
Kapton	Elastic modulus (N/m^2)	$+2\% = 2.8152 \times 10^9$	9687658	0.009290188
		$-2\% = 2.7048 \times 10^9$	9687650	-0.005161216
	Poisson's Ratio (-)	$+2\% = 0.3468$	9603607	0.867424884
		$-2\% = 0.3332$	9768592	-0.835621472
CFRP	Elastic modulus (N/m^2)	$+2\% = 1.326 \times 10^{11}$	11657041	0.008149594
		$-2\% = 1.274 \times 10^{11}$	11657027	-0.00214463
	Poisson's Ratio (-)	$+2\% = 0.102$	11644495	0.107463124
		$-2\% = 0.098$	11669527	-0.107274396

Table 5.3: Uncertainty in material properties with sensitivity index shown for maximum stress values

In Table 5.3, only the results for Elastic Modulus and Poisson's Ratio are presented because all other material properties produced a sensitivity index of 0. Across all four materials, the following uncertainty percentages were applied: 2% (Elastic Modulus, Poisson's Ratio and Shear Modulus), 1% (Mass Density) and 5% (Tensile Strength, Compressive Strength, Yield Strength, Thermal Expansion Coefficient, Thermal Conductivity and Specific Heat).

Conclusion: This section provided results for models made up of sixteen Miura unit cells, which, when fully deployed will produce a single flat rectangular panel. The panels of the net of a pyramidal horn antenna are trapezoidal and this shape can be achieved simply by adding or removing some Miura unit cells. Four of these panels can then, at a certain angle, unfold in order to create the shape of a pyramidal horn antenna.

6 Discussion

This section provides a critical analysis of the method employed in light of the results, as well as situating the project in a broader context.

6.1 Methodology limitations

The methodology used to obtain the results for this dissertation has several limitations, which will be discussed in this subsection.

The models used for testing in the Solidworks simulations were scaled down prototypes, scaled to roughly a tenth of the expected full size of the horn antenna for the radio telescope. In the results section, it is suggested that stress distributions for different geometries and materials provide an indication of an ideal solution and the validity of this method can easily be tested in real life using models manufactured in a laboratory. However, stress distributions do not necessarily scale linearly with an increase in model size, therefore, the ability to experimentally recreate this method in a laboratory on a full scale model (roughly $10 \times 10 m$) would allow one to determine whether the results in Section 5 can simply be scaled up.

When creating models 1 to 5, only five $b : a$ ratios were considered. Although it would be impossible to create a model for every existing ratio of lengths, only five configurations were considered. This gave the general trend of stress distribution and $b : a$ ratio, although a more thorough approach (considering more than five initial models) could have revealed the ideal ratio to be approximately $1 : 1$, with a small variation, resulting in a more accurate ‘ideal’ geometry.

When considering materials used, the results for the first ten models are reliable, as they were made of foamboard, whose material properties were found in the Solidworks database pre-set in the software, based on industry standards. These material properties correspond to the standard paper-faced polystyrene foamboard, although there are many different types, meaning a limitation of using this default setting in the methodology is that creating models in a laboratory to test them experimentally would require the use of that specific type of foamboard only, to ensure validity of results comparison.

Regarding models 11 to 14, which are made of other materials, their material properties were based on relevant literature, which would often provide a range of values. The average value was taken and a sensitivity analysis was performed on all material properties for each of the four materials. The uncertainty percentages used in this sensitivity analysis were based on industry standards, given in the references provided, however, these did not consider the exact method being applied with the materials. A lower uncertainty percentage would have resulted in all material property values producing a sensitivity index of 0, whereas a high uncertainty percentage would have resulted in an increased sensitivity index for all material properties. The trade off between uncertainty in the chosen values and sensitivity index was not directly considered, which posed a limitation on the effectiveness of this quantitative analysis. Another major limitation in relation to use of material is that each model was made entirely of one material. It is common in engineering applications for space structures to be made of several different materials, as each element of the structure has different flexibility, stiffness and strength requirements. Using more than one material is a simple solution to providing the necessary properties to all components of the structure. The use of only one material for each model in this project imposes the creation of monolithic structures, without the consideration of different materials for hinges or areas of significantly higher stress. As well as this, the assumption made by Solidworks is that the material properties are homogeneous and isotropic throughout the entire model. This is a limitation because this assumption is not applicable to real life examples, since in general, factors such as grain structure, defects and material density can have small variations throughout the material, which could cause stress concentrations or localised deformations in the results.

A large limitation when considering the FEA simulations is that only one configuration of fixtures and external loads was used consistently throughout all results. This provided the most realistic approximation of the deployment process that would have occurred in laboratory conditions and produced results showing desirable displacement trends for the forces and fixtures set. A limitation with this part of the methodology is that applying a force on the panel faces rather than the panel edges eliminates the possibility of certain deployment methods mentioned in section 3.3. Practical applications of these simulations might require a force to be applied on all hinges,

other specific edges of the model or on certain sections of panel faces, which would completely change the results obtained. In real world scenarios, the angle at which this force is applied and the planes on which the panels are fixed can vary, therefore only considering one configuration is unlikely to be fully representative of what the results are aiming to demonstrate, despite ensuring consistent results.

A blended curvature based mesh was used for good computational efficiency, whilst ensuring a very high level of accuracy in the results, however, this mesh type in Solidworks sometimes struggles to capture deformations in areas of high stress when using thin models. Section 5.4.1 details the mesh convergence technique applied in order to counteract this limitation.

6.2 Critical analysis of results

From the results in section 5.1, it can be seen that as $b : a$ ratio decreased from 1:1, maximum stress increased and the overall stress became less uniformly distributed across the model. The stress also shifted from being more concentrated on top edges to being more concentrated on the side edges, as well as more stress near the fixed panels rather than the panels being ‘pulled’. As the $b : a$ ratio increased, the opposite was observed, with stress becoming highly concentrated at the top edge of the nearest panel (on which force was applied), especially for model 4, which has the highest ratio. The stress for models 1 and 5 were both even distributed, relative to other models, however in general, stress on the edges in model 5 was higher, making it a less desirable solution comparatively. Regarding strain, as $b : a$ ratio increased, strain decreased. The same trend in the change in stress distribution between models was observed for strain. The displacement plots indicate the amount of deployment achieved for a given force applied, as well as suggesting the deployment directions. For high and low $b : a$ ratios, deployment (or ‘flattening’) of the model is uni-axial because one end of the models can be seen to have the highest displacement. For model 1 with a ratio of 1:1, the displacement distribution is applied diagonally across each Miura unit cell, proving that this model will deploy evenly in both x and y axes, rather than mainly in one direction. A higher $b : a$ ratio resulted in a lower overall displacement of all elements, meaning a larger force would be required for those models to result in the same displacement

as lower $b : a$ ratio models. These results imply that it is advantageous to have a folded horn antenna, as long as the $b : a$ ratio is 1:1. This is because at this ratio, the geometry does not create directional limitations when considering deployment and the stress distribution is uniform, without extreme values at the edges or fold lines (where hinges could be placed), making model 1 a more feasible solution compared to models 2 to 5.

Section 5.2 pictures results for models 6 to 10 which show that an increase in model thickness corresponds to a decrease in maximum stress, however, at the higher thicknesses, higher stress values become more concentrated along the entire edge of fold lines, rather than at one small point. For a given applied force, thinner models had a higher maximum stress but less failure points than thicker models. As thickness increased, strain also decreased because thicker structures have more stiffness. The results show that the thinner models were less able to resist bending than the thicker ones for foamboard. The strain distribution remained relatively the same across these models, since the geometry remained unchanged. The displacement plots for the models shown in section 5.2 show an exponential decrease in maximum displacement as thickness increases, meaning that to achieve the same displacement (and therefore amount of deployment), thicker models would require more force, as thinner models are more compliant. These results imply that it is advantageous to have a folded horn antenna with a thinner structure because it would require less overall force to fully deploy and would contribute less mass to the mass budget of the system. Thinner horn antenna panels would also have less failure points due to a more uniform stress distribution.

All four materials simulated in section 5.3 showed similar stress distributions, however for a given structure, applied force, fixture and mesh configuration, CFRP had the highest maximum stress, followed by Nitinol, Kapton and PEEK. The materials also had similar strain distributions, as this is largely determined by geometry and simulation setup. They highlighted the most strain in the middle of the fixed panels because of small internal deformations, which occur due to the models being thin structures. CFRP displayed the least amount of maximum displacement, followed by Nitinol, Kapton and PEEK, which reflects the maximum stress value trend. These materials are all examples of innovative materials that could have applications

to foldable horn antennas. The choice of material would depend on the system requirement of the overall mission and deployment methods. As mentioned in section 6.1, a combination of these materials could also be used in order to leverage the advantages that they provide to the structure.

6.3 Links to broader engineering context

The development of origami-inspired space structures has resulted in an enormous contribution to the space industry's research and advancements, especially in the last decade. It provides a solution to mass and volume constraints when transporting large structures into space and implementing foldable components on space missions is becoming more prevalent in applications where compactness and rapid deployment are desirable, such as solar arrays, mirrors and sun shields. This concept also has many applications on Earth, for example it can be used for mobile shelters in war zones or collapsible bicycles. Currently, the trend for space technology is creating small lightweight structures without compromising on performance, a common example being CubeSats. Introducing a foldable solution would ensure this portability, as well as having the duality of being a deployable system, with applications in search and rescue antennas for emergencies.

A previous example of an origami-based horn antenna is the FH-1E (Farr et al. 2007), which includes parabolic bends in the feed section, reducing the depth of the antenna, without affecting the aperture section. The work in this dissertation investigates the application of bends in the aperture section as well, since the fully deployed design is much larger than FH-1E and operates in a higher frequency band. Rather than focusing on increasing aperture efficiency, this project aims to optimise the geometry of the horn antenna aperture panels in order to achieve a physically feasible model.

7 Conclusion

The investigation carried out in this project is important because it addresses a large gap in current research. As of 2025, very few origami horn antennas have been developed, none of which were specialised for use on a radio telescope. This project has explored the effects of different geometries, thicknesses and materials on foldable models of horn antenna aperture plates, proving the feasibility of folding them, based on stress and strain variation. The less common materials chosen for investigation suggest that the standard approach of using aluminium or steel may not be the only solution, as they do not have ideal properties for deployment. This dissertation demonstrates that it is viable to manufacture a scale model of a pyramidal horn antenna's foldable aperture plates for a radio telescope, using an origami-inspired pattern which is optimised for favourable stress, strain and displacement distributions. Full scale practical experiments would need to be done in order to develop the specific deployment method and to test the performance of the antenna once all foldable elements are fully deployed. Further related study would also include testing different deployment configurations to examine the effect of fixtures on deployment capability or using more than one material for foldable structures to optimise performance, mass, cost and functionality. Optimising the total mass of a large space structure could also be achieved by 'hollowing out' certain panels. Especially for radio telescope applications where horn antennas act as feeds for large wavelength signals, holes could be created in these panels, with dimensions less than that of the wavelength of signals being collected, essentially removing unnecessary material.

As mentioned in section 6.3, outcomes of this research could enable the development of foldable search and rescue antennas for aircraft, ships or ground vehicles for use in emergency situations, where portability is crucial. For these applications, more research would need to be done to ensure the use of robust materials, however the structural design discussed in this project would provide the necessary compactness and quick deployability required for such missions. This origami horn antenna design could also be used in the defence industry for communication or tracking and it could be adapted to have a varying aperture size for missions with different operating frequencies, whilst being portable and durable.

Since this project has focused on the optimisation of one panel made of sixteen Miura unit cells, this can be modified into many different shapes for use outside of this research area. For example, the design of the hinges for deployable emergency shelters could take inspiration from the origami pattern investigated in this project, since reduced stress on the bent part of the material would improve the lifetime of the product and allow an increased number of folding and unfolding cycles, making the mobile shelters last longer. Removing the need for extra tools for setup would also ensure faster deployment during a crisis. This could also be applied to most packaged consumer products due to the panel's collapsible feature - this could create items such as reusable water bottles, which would align with current sustainability trends and help to reduce negative environmental impacts. Furthermore, this origami-inspired design could enable STEM outreach events at schools, to teach young people about the space sector's technological advancements and to allow them to understand the technical principles behind horn antennas through a hands on learning experience.

The data collected for a radio telescope requires precise and seamless integration of all panels of a pyramidal horn antenna and simultaneously eliminating creases from folding to ensure the internal smoothness of the panels. One solution to this would be developing magnetic latching joints that mimic self-aligning hinges. This would need to be simulated in order to test repeatability of deployment and folding. The findings of this report imply that smart materials with properties desirable for horn antennas, such as high conductivity or good corrosion resistance can feasibly be folded into a compact Miura folded design, presenting the opportunity for more passive or automated deployment methods to be developed. The FEA analysis done on this specific 3D pattern enables the comparison of failure modes and fatigue, facilitating the identification of chosen material for a specific mission's system requirements.

Appendix A

Project Plan

Initial Plan

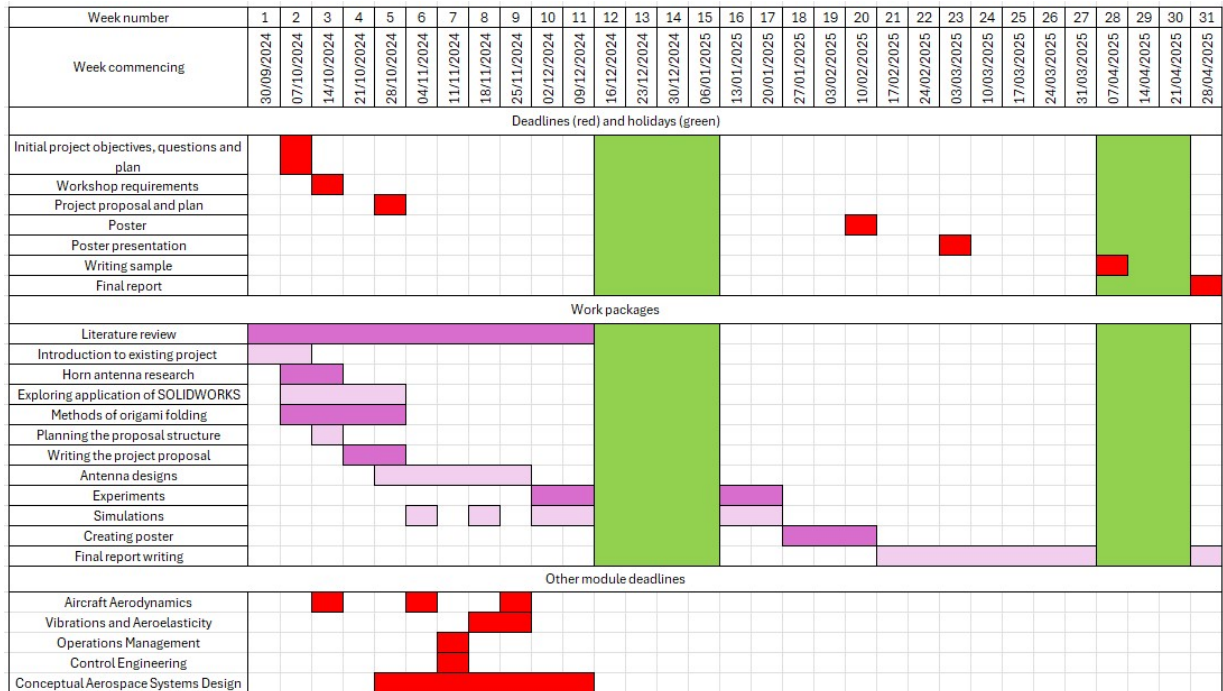


Figure 7.1: Initial gantt chart created in week 2

The initial gantt chart was created before this project was started, therefore certain work packages were not made very clear and there was a lot of overlap between them. The deadlines were also ambiguous as to the exact due dates and type of deadline, since one piece of coursework cannot be due for an entire week.

First Revised Plan

Upon receiving feedback from the first deliverable, the initial gantt chart was amended. At this point, the project had been introduced and this added clarity, allowing the work packages to be defined more clearly. Specific due dates and times were also added to the deliverables for this individual project. The extra work packages for semester 2 had not yet been added, as this was decided near the end of semester 1, depending on progress made.



Figure 7.2: Project proposal gantt chart with clearer work packages and detailed due dates for project deliverables

Figure 7.2 is a gantt chart for semester 1 that shows all the other module deadlines, with their specific due dates and times. To manage year 3 workload, these deadlines were considered when creating the amended gantt chart and it can be seen that less work packages have been allocated to week 7, where there are several deadlines for other modules.

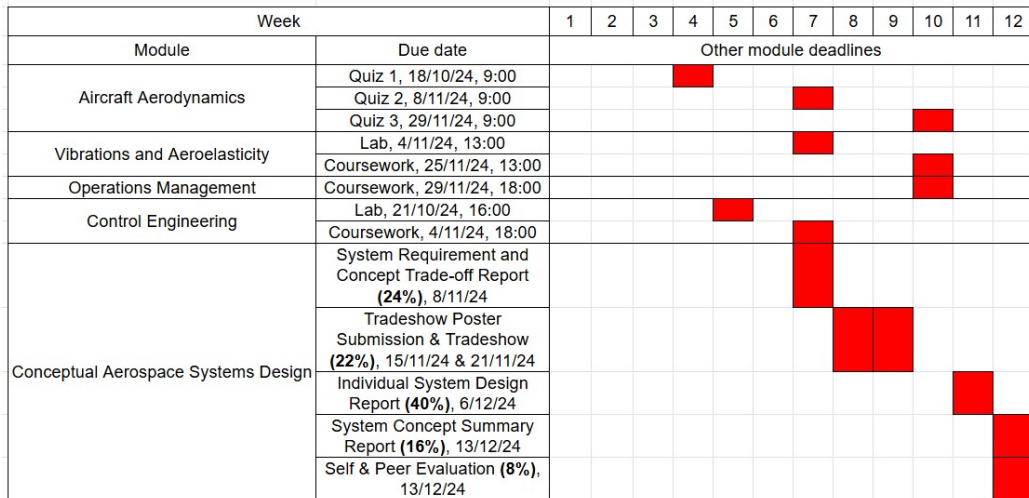


Figure 7.3: Gantt chart for other module deadlines for semester 1

To ensure efficient time management, a further spreadsheet was created that is linked to the semester 1 revised gantt chart. This lists how many hours are intended to be spent on each work package per week and this is compared to how many hours were actually spent. The spreadsheet was be updated every Sunday by the end of the day and this document was accessible to the project supervisor.

Notes were inserted where appropriate to give reasons as to why more or less time than intended was spent on certain work packages. This will be useful for guiding

any potential changes to this spreadsheet in the further weeks of semester 1, as this unit is worth 30 credits. 10 credits' worth is allocated this semester, equating to 100 hours of work to be spent on it in the first 12 weeks. This method of time management will ensure enough work is put into the project, as well as increasing visibility to the project supervisor and easing progress-related communication.

Plan for Semester 1		current week											
Week:	Task	1	2	3	4	5	6	7	8	9	10	11	12
	Hours to spend	Actual hours spent	Hours to spend										
Supervisor meetings	1	0	0	0	0.5	0.5	0	0	0.5	0	0	0.5	0
Introduction to project	0.5	0.5	1	0	0	1	0	0	0.5	0	0	0	0
Writing initial project plan	0	0	1	0.5	2	2	0	0	0	0	0	0	0
Exploring potential software	0	0	2	2	1	1	0.5	1	0	0	0	0	0
Exploring application of Solidworks	0	0	0	0	2	3	0	0	2	0	0	1	0
Literature review	0	0	2	3	2	2	2	0	0	3	0	2	0
Planning the proposal structure	0	0	0	0	0	0	1	1	0	0	0	0	0
Time management	0.5	0.5	0.5	1.5	1.5	0.5	0.5	1	3	0.5	1	0.5	0.5
Writing the proposal	0	0	0	0	1	3	1	4	14	2	1	0	0
Simulations	0	0	0	0	0	0	0	0	0	0	2	0	3
Experiments	0	0	0	0	0	0	0	0	0	1	0	2	0
Total weekly hours:	2	1	6.5	7	10	10	6	2.5	8.5	23.5	2.5	5	1
Total hours to spend:	73												
Total hours actually spent:	49												

Figure 7.4: Spreadsheet detailing number of hours to spend vs number of hours actually spent on work packages every week and includes notes to explain deviations from expected hours (to be updated weekly)

Second revised plan

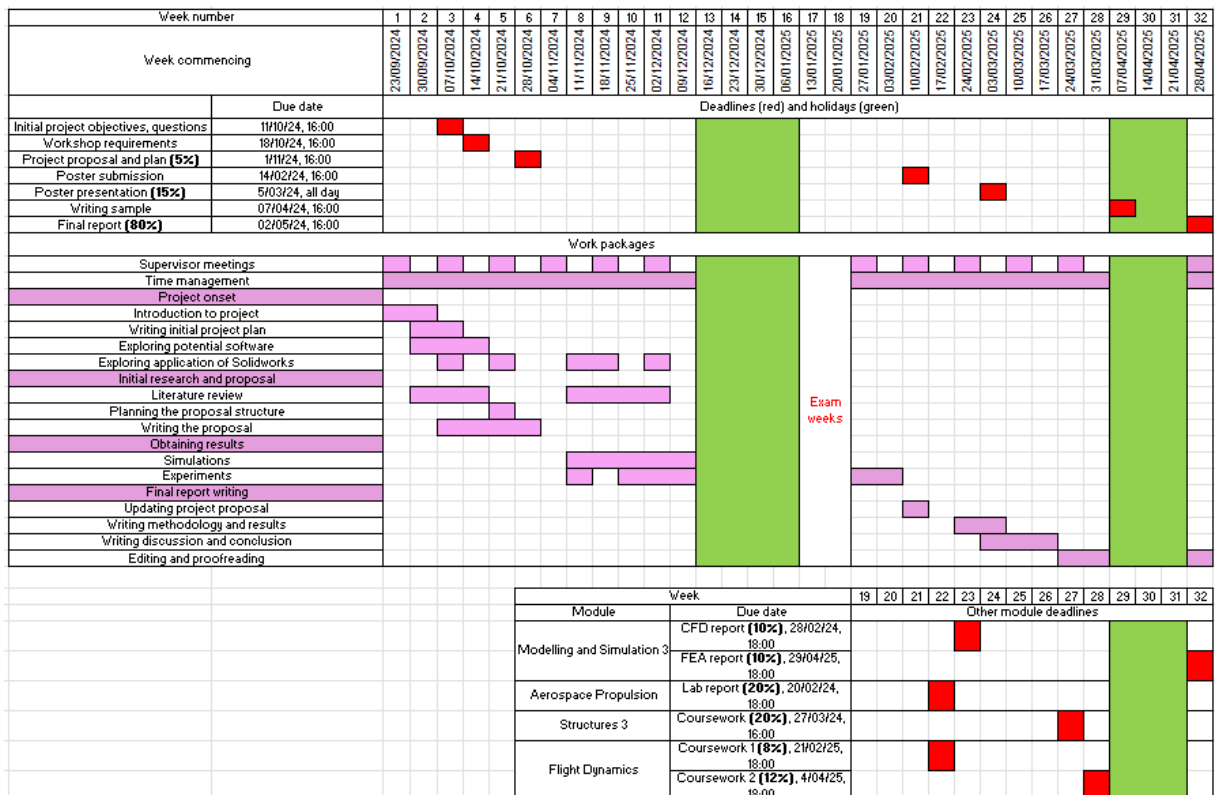


Figure 7.5: Second revised plan created in week 17

Upon receiving feedback on the project proposal, the second revised plan was created at the beginning of semester 2, with work package headings. The second semester deadlines for other modules were also added alongside this gantt chart, with less dissertation work scheduled during weeks containing several other deadlines in order to manage workload. Exam revision was prioritised during the two exam weeks in January.

Final detailed plan

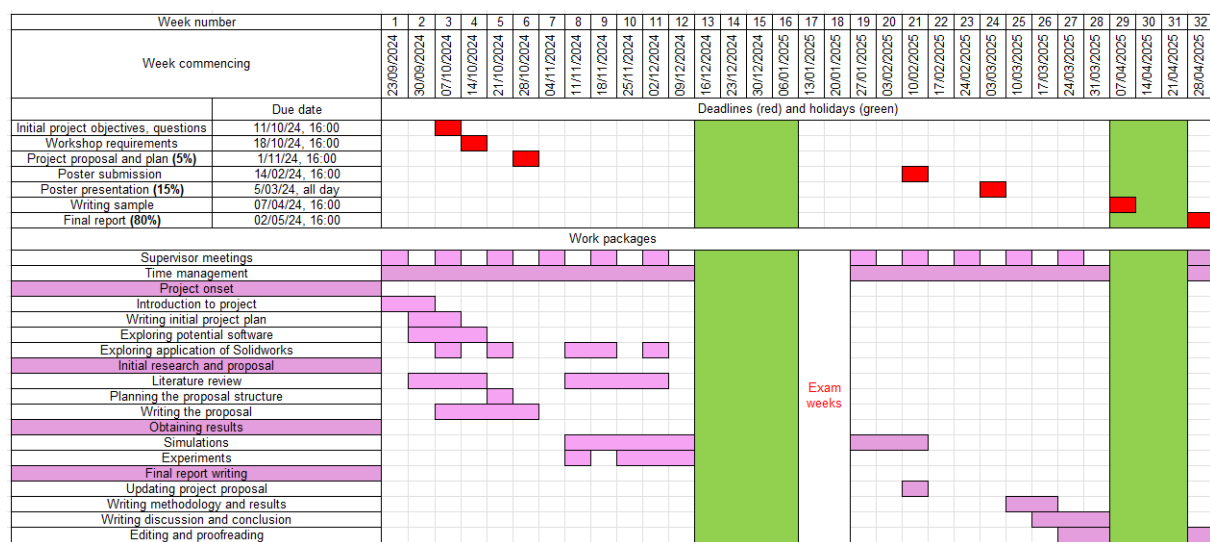


Figure 7.6: Final detailed plan created at the end of the project

This final plan details the actual amount of work spent on each work package throughout the entire year. Solidworks simulations took longer than expected, meaning there was no time to completely build the test rig for practical experiments, despite having ordered parts, created a foamboard model and developed a risk assessment. Although the experiments could not be completed as part of this project, future projects could utilise the items ordered, providing them with a starting point for the experimental testing of foamboard origami models.

Appendix B

Risk Management

Laptop breaks

The main device on which this individual project is being written is a personal Lenovo laptop but there is a problem with its hinge and there is a chance the screen might crack and stop working, as it did two years ago. Writing up this document in Latex would remove any issues if this laptop were to break, as this Overleaf account can be accessed from any device, meaning the report write up could be continued on any university computer until this device is fixed.

Issues with lab access

In order to make the models detailed in the Methodology section, regular access to the UAV laboratory on the ground floor of Engineering Building A is required - this is not an area to which students have access. In order to mitigate this risk, the relevant department was spoken to and access was granted through an update to the student ID card.

No material access

As detailed in previous sections, foamboard is required to make the models for experiments, however this is only available through the university and there is a risk that none will be available as soon as needed. A precaution to take is to put in an early request at the next GFA meeting to use some foamboard sheets. Foamboard is stored on the sixth floor of Engineering Building A and this storage space can be visited upon requesting permission from previous internship employer.

Time Management

Since there are several other modules with deadlines each week, it is easy to fall behind in this individual project if time is not managed correctly and frequently. This can be avoided by adhering to the gantt charts and spreadsheet outlined in this appendix. Updating these weekly to ensure staying on task will result in good time management. Future projects could also consider creating conical horn antennas using the same methodology provided in this report.

References

- Aboserwal, Nafati Abdasallam (2014). "Gain and Loss Factor for Conical Horns, and Impact of Ground Plane Edge Diffractions on Radiation Patterns of Uncoated and Coated Circular Aperture Antennas". PhD thesis. Arizona State University.
- Alarcón López, Susana (2017). *DuPont Kapton Summary of Properties*. Tech. rep. DuPont.
- Alipour, S. et al. (2022). "Nitinol: From historical milestones to functional properties and biomedical applications". In: *Journal of Engineering in Medicine*.
- Beyer, Matthew T., Alec D. Figler, and Kevin Owen (2023). "'Origami' Horn Antenna for Contactless Vital Sign Monitoring". In: *LIBRAETD*.
- Caldecott, R. et al. (Jan. 1973). *HIGH PERFORMANCE S-BAND HORN ANTENNAS FOR RADIOMETER USE*. Tech. rep. NASA.
- Crawford, A. B., D. C. Hogg, and L. E. Hunt (1961). "A Horn-Reflector Antenna for Space Communication". In: *The Bell System Technical Journal*.
- Deleo, Antonio Alessandro et al. (2020). "Origami-based Deployable Structures Made of Carbon Fiber Reinforced Polymer Composites". In: *Composites Science and Technology*.
- Farr, Everett G. et al. (2007). "The Folded Horn Antenna". In: *Transactions on Antennas and Propagation*.
- Gabauer, W. (2000). "Manual of Codes of Practice for the Determination of Uncertainties in Mechanical Tests on Metallic Materials". In: *Standards Measurement and Testing*.
- Granet, Christophe and Graeme L. James (2005). *Design of Corrugated Horns: A Primer*. IEEE Antennas and Propagation Magazine.
- Grosvenor, Chriss A. et al. (Jan. 2007). *TEM Horn Antenna Design Principles*. NIST Publications.
- Gupta, Divya (Jan. 2014). "DESIGNING OF THE CONICAL CORRUGATED HORN ANTENNA". In: *International Journal of Scientific and Engineering Research* 5.
- Hunter, Colin, Avinkrishnan Vijayachandran, and Anthony M. Waas (2023). "Self-deployable hinges for monolithic space structures using multi-material additive manufacturing". In: *Elsevier*.
- Kalra, Sahil et al. (Mar. 2019). "Investigations on the suitability of PEEK material under space environment conditions and its application in a parabolic space antenna". In: *Elsevier*.
- Kshirsagar, Mohit et al. (Oct. 2023). "Origami engineering: Creating dynamic functional materials through folded structures". In: *Elsevier*.
- Kumar, R., R. Singh, and A. Sharma (2021). "Mechanical properties of carbon fibre reinforced polymer composites: A review". In: *Science Direct*.
- Li, Mengyue et al. (2023). "Design and deformation analysis of an inflatable metallic cylinder based on the Kresling origami pattern". In: *Elsevier*.
- Lu, Lu et al. (2021). "Conical Kresling origami and its applications to curvature and energy programming". In: *Royal Society Publishing*.
- Ma, Shuo et al. (2021). "Design and analysis of deployable clustered tensegrity cable domes". In: *Proceedings of the IASS Anual Symposium 2020/2021*.
- Morgan, Jessica, Spencer P. Magleby, and Larry L. Howell (2016). "An Approach to Designing Origami-Adapted Aerospace Mechanisms". In: *ResearchGate*.

- Moshtaghzadeh, Mojtaba et al. (Mar. 2022). "Artificial Neural Network for the prediction of fatigue life of a flexible foldable origami antenna with Kresling pattern". In: *Elsevier*.
- Nikolova (n.d.). "Horn Antennas (Rectangular Horn Antennas, Circular Apertures)". McMaster lecture notes.
- Okuzumi, Nobukatsu and Takaya Yamamoto (2009). "Centrifugal Deployment of Membrane with Spiral Folding: Experiment and Simulation". In: *Journal of Space Engineering*.
- Penzias, Arno A. and Woodrow R. Wilson (1964). "Horn Antenna, Holmdel, N.J." In: *Library of congress*.
- Schenk, Mark and Simon D. Guest (Jan. 2013). "Geometry of Miura-folded metamaterials". In: *PNAS*.
- Seigner, Lena et al. (2020). "Origami-Inspired Shape Memory Folding Microactuator". In: *Proceedings*.
- Singh, Jashanpreet and Amandeep Singh Dhaliwal (Dec. 2011). "Optimization and Designing of Conical Horn Antenna". In: *IJECT*.
- Singh, Thakur Pranav G. et al. (2024). "A Novel Non-Pyrotechnic Radial Deployment Mechanism for Payloads in Sounding Rockets". In: *Theoretical and Applied Mechanics Letters*.
- Skirbutis, G. et al. (2018). "PEEK polymer's properties and its use in prosthodontics. A review". In: *Stomatologija, Baltic Dental and Maxillofacial Journal*.
- Soares, Pedro A. G., Pedro Pinho, and C. A. Wuensche (2014). "High performance corrugated horn antennas for CosmoGal satellite". In: *Elsevier*.
- Wagner, R. and H. M. Braun (1980). "A slotted waveguide array antenna from carbon fibre reinforced plastics for the European space SAR". In: *Acta Astronautica*.
- Walker, M. G. and K. A. Seffen (Sept. 2018). "The Mechanics of Metallic Folds". In: *Word Press*.
- Wang, Xin et al. (2024). "In-Plane Small-Deformation Equivalent Method for Kinematic Analysis of Tubular Miura-Ori". In: *The Chinese Society of Theoretical and Applied Mechanics*.
- Wei, Qiang et al. (2018). "Effects and mechanism on Kapton film under ozone exposure in a ground near space simulator". In: *Elsevier*.
- Xia, Wei et al. (Jan. 2023). "Optimal Design and Experimental Study of Horn Antenna in Pavement Microwave Deicing Technology". In: *Cold Regions Science and Technology*.